Resistance model uncertainty in non-linear finite element analyses of cyclically loaded reinforced concrete systems

RESISTANCE MODEL UNCERTAINTY IN NON-LINEAR FINITE ELEMENT ANALYSES OF CYCLICALLY LOADED REINFORCED CONCRETE SYSTEMS

Paolo Castaldo[1], Diego Gino[1], Gabriele Bertagnoli[1], Giuseppe Mancini[1]

[1]Department of Structural, Geotechnical and Building Engineering (DISEG), Politecnico di Torino, Turin, Italy. E-mail: paolo.castaldo@polito.it; diego.gino@polito.it; gabriele.bertagnoli@polito.it; giuseppe.mancini@polito.it

Corresponding Author

Castaldo Paolo

paolo.castaldo@polito.it

(pcastaldo@unisa.it)

+39 0110905307

RESISTANCE MODEL UNCERTAINTY IN NON-LINEAR FINITE ELEMENT ANALYSES OF CYCLICALLY LOADED REINFORCED CONCRETE SYSTEMS

Paolo Castaldo[1*], Diego Gino[1], Gabriele Bertagnoli[1], Giuseppe Mancini[1]

[1]Department of Structural, Geotechnical and Building Engineering (DISEG), Politecnico di Torino, Turin, Italy. (**corresponding author*) E-mail: paolo.castaldo@polito.it; diego.gino@polito.it; gabriele.bertagnoli@polito.it; giuseppe.mancini@polito.it

ABSTRACT

This study assesses the partial safety factor corresponding to the resistance model uncertainties in the use of non-linear finite element analyses (NLFEAs) for reinforced concrete systems subjected to cyclic loads. Specifically, various walls experimentally tested are considered for this investigation and are simulated through two-dimensional (i.e., plane stress) finite element (NLFE) models. The comparison between the global resistances from the plane stress NLFE structural models and the experimental tests is carried out considering the possible modelling hypotheses available in relation to the mechanical response of reinforced concrete structural systems subjected to cyclic loads. After that, a probabilistic processing of the abovementioned epistemic uncertainties is carried out in line with a Bayesian updating. In detail, each prior distribution of the resistance model uncertainty related to a specific combination of the modelling hypotheses is computed and successively updated with the data achieved from the other models to estimate the posterior distribution. Hence, the coefficient of variation and the mean value of the resistance model uncertainties are evaluated and the corresponding partial safety factor is assessed in line with the NLFEA safety formats of reinforced concrete systems for seismic analyses.

KEYWORDS: non-linear finite element analysis; resistance modelling uncertainties; partial safety factors; reinforced concrete systems; Bayesian updating; plane stress; cyclic loads.

1. INTRODUCTION

The evaluation of the structural behaviour of reinforced concrete (RC) systems in different loading configurations is a primary aspect in order to ensure durability, functionality (i.e., serviceability limit states) and safety (i.e., ultimate limit states). Advanced tools, as non-linear finite element analyses (i.e., NLFEAs), have become one of the most common solutions for the design of complex new RC structures and also for the assessment of existing infrastructures and structures (e.g., bridges and viaducts).

Generally, a non-linear NLFE structural model needs an appropriate validation and calibration process [1]-[4]. In order to use NLFEAs for the design or assessment of RC systems, the numerical outcomes should be appropriately analysed and post-processed in order to fit the reliability criteria prescribed by Codes [5]-[9]. To this aim, several methodologies, denoted as safety formats, have been introduced by the scientific literature [10]-[13] and standards [5],[14]. Discussions about the global safety formats for NLFEAs of RC systems may be found in [15]-[18]. In [19], a discussion of the different safety formats with the proposal of an additional safety factor in order to account for its dependence on the alteration of the failure mode is presented. All the mentioned above safety formats provide a framework devoted to assess the design value of the global structural response (e.g., global resistance) considering two different types of uncertainties [20]: the aleatory uncertainties affecting both the material properties and geometry, and the epistemic ones related mainly to the assumptions performed within the definition of the NLFE model. Concerning the uncertainty related to material properties and geometry, information about their inherent variability is widely provided by the scientific literature, whereas information relating the uncertainty associated to NLFEAs resistance models is complex to be evaluated [20], in particular, when the

structural models are subjected to cyclic loads. In fact, any NLFEA is based on specific hypotheses which can influence the final numerical result in comparison to experimental outcome [20]. In this context, JCSS Probabilistic Model Code [21] provides useful recommendations in order to consider the resistance model uncertainties for reliability analyses in static conditions, in particular, concerning bending and shear behaviours. In [22], a study focused on the evaluation of model uncertainties related to slabs and punching failure is presented. In [20] and [23], the resistance NLFEA uncertainties are taken into account considering the experimental tests with different behaviours and failure modes. However, any information is not available in literature regarding structural systems subjected to cyclic loads.

This study, in line with the approach of [20], proposes the estimation of the resistance model uncertainty partial safety factor related to NLFEAs of RC systems subjected to cyclic loads for seismic analyses. The mentioned above partial safety factor is in line with the methodologies described by the global safety formats for NLFEAs defined by [5]. Specifically, various experimental test sets related to shear walls with the outcomes reported by the scientific literature are herein considered. In particular, 17 experimental tests on shear walls subjected to in-plane cyclic loading have been selected from the results of several authors [24]-[28]. The literature proposes also results concerning experimental and numerical characterization RC shear walls in case of out-of-plane cyclic loading process [29]-[31]. However, the present investigation is focused on estimation of resistance model uncertainty in plane stress numerical models and so only experimental tests with in-plane loading process are considered for the probabilistic calibration of the associated resistance model uncertainty partial safety factor with reference to a specific level of reliability. In agreement with [20], each experimental result has been numerically reproduced adopting different modelling hypotheses to estimate the resistance model uncertainties associated to the seismic response of various RC members. Specifically, the uncertainty in definition of plane stress NLFE resistance models is estimated defining eighteen structural models which differ in the software platforms and in the mechanical laws to simulate the response of concrete (i.e., modelling hypotheses [20],[32]). Hence, a comparison in terms of the peak global structural resistance between the numerical outcomes (i.e., plane stress configuration) and the experimental data is carried out. Next, a probabilistic processing of the abovementioned epistemic uncertainties is performed with a Bayesian approach, as proposed in [20], in order to evaluate the most appropriate probabilistic distribution with the related statistical parameters (i.e., variance and mean), able to represent the resistance model uncertainty. Successively, in compliance to [5],[14],[20], the resistance model uncertainty partial safety factor for NLFEAs of RC systems subjected to cyclic loads for seismic analyses is assessed accounting for different target reliability indices [5],[8],[9] in relation to existing or new RC structures, direct and indirect consequences of failure and residual/design service life. Moreover, the partial safety factors are evaluated assuming the hypotheses of dominant or non-dominant random variable as widely discussed in [20].

2. EVALUATION OF THE EPISTEMIC UNCERTAINTY IN THE RESISTANCE MODEL DEFINITION AND OF THE RELATED PARTIAL SAFETY FACTOR

As previously discussed, both aleatory and epistemic [32]-[35] families of uncertainties are involved in structural engineering. Concerning the aleatory uncertainties, they are represented by the variables for which the inherent randomness cannot be affected or reduced by external (i.e., human) intervention as it is an intrinsic characteristic of the structure or of the physical properties. Instead, it is referred to the epistemic uncertainties when an increase of the knowledge about the specific problem may lead to a significant reduction of the level of uncertainty. In detail, they may be represented by the choices performed for the definition of a structural model (i.e., modelling hypotheses) and, for example, by the assumptions regarding auxiliary non-physical parameters [32]. The methodologies defined with the purpose to perform the design and assessment through NLFEAs have to account for both the mentioned above families of uncertainties.

In line with the global safety formats for NLFEAs proposed by Codes and literature [5],[10],[11],[14], the global design structural resistance R_d can be evaluated as follows:

$$R_d = \frac{R_{rep}}{\gamma_R \gamma_{Rd}} \tag{1}$$

where R_{rep} denotes the representative value (in compliance to the selected safety format [5]) of the global structural resistance (i.e., the peak response in cyclic analyses) evaluated using NLFEAs; γ_R is the global resistance partial safety factor and accounts for the aleatory uncertainty related to material properties; γ_{Rd} denotes the resistance model uncertainty partial safety factor which accounts for the epistemic uncertainty related to the definition of the non-linear structural model.
NLFEAs on RC systems under a cyclic loading process (e.g., seismic analysis) may present larger levels of modelling uncertainties if compared to the static case. For instance, an appropriate and reliability-based assessment of the partial safety factor γ_{Rd} is necessary. To this purpose, the methodology proposed by the same authors in [20] is adopted for the calibration of the resistance model uncertainty partial safety factor γ_{Rd} related to plane stress NLFEAs under cyclic loads. In compliance with [5],[10],[20]-[21],[38]-[40], the resistance model uncertainty random variable, denoted as ϑ, can be represented by the following ratio:

$$\vartheta = R\,(X,Y) / R_{NLFEA}(X) \tag{2}$$

where $R(X,Y)$ is the global structural resistance obtained through the experimental investigation, whereas $R_{NLFEA,}(X)$ is the global structural resistance achieved through a NLFEA. The vector X groups all the relevant variables which are explicitly accounted for during the definition of the structural model and the vector Y accounts for neglected physical and non-physical variables that may have some influence on the actual structural response. The global structural resistance, estimated through both experimental and numerical tests, is herein intended as the peak load achieved in cyclic analyses in line with the global force-based approach of safety formats for NLFEAs. The definition of a NLFE structural model, as will be discussed in the next sections, requires to perform choices between different possible modelling hypotheses [23]. These different assumptions (e.g., related to material models, convergence criteria, numerical approximations and type of finite elements) may lead to diverse structural models which may be used by engineers and it can happen that each structural model representing the same structure may provide different results. So, an appropriate characterization of the probabilistic model able to represent the random variable ϑ is necessary. According to [21], a lognormal probabilistic distribution can be efficiently adopted in order to describe the statistical variability of the realizations of the variable ϑ conditional to several plausible modelling hypotheses (i.e., prior distributions). Hence, following the procedure described by [20], a Bayesian updating can be used in order to define the average distribution representing the resistance model uncertainty random variable ϑ with the related statistical parameters (i.e., mean value μ_ϑ and standard deviation σ_ϑ.). In line to [21],[38]-[41], with the assumption of lognormal probabilistic distribution, the resistance model uncertainty partial safety factor γ_{Rd} may be evaluated as:

$$\gamma_{Rd} = \frac{1}{\mu_\vartheta} \exp(\alpha_R \beta V_\vartheta) \tag{3}$$

where V_ϑ represents the coefficient of variation (COV) of the random variable ϑ estimated as $\sigma_\vartheta / \mu_\vartheta$; the first-order-reliability-method (FORM) sensitivity factor for the resistance variables α_R can be assumed equal to 0.32 and 0.8 [5],[14],[42] accounting for the hypothesis of non-dominant and dominant variables, respectively; the term β denotes the target reliability index [42].

In the following, the results of several experimental tests concerning shear walls subjected to in-plane cyclic loading processes are considered. Each experimental test set is simulated through plane stress NLFEAs considering different modelling hypotheses to evaluate the resistance model uncertainty random variable ϑ. Finally, the related partial safety factor for NLFEAs of systems subjected to a cyclic loading process for seismic analyses is evaluated.

3. MODELLING HYPOTHESES FOR NLFEAs AND NUMERICAL RESULTS

This section describes various walls subjected to in-plane cyclic loads [24]-[28] and the NLFEAs performed by the authors after a sensitivity/calibration analysis to reproduce the experimental tests. The numerical simulations are defined in compliance with different modelling hypotheses to estimate the resistance model uncertainty random variable and the related partial safety factor as stated by the global safety formats for NLFEAs [5] for design or verification aims within the seismic field. In fact, the results from structural analyses carried out throughout NLFEAs are always affected by numerical errors due to iterative calculation procedures to respect the fundamental mechanics principles: equilibrium, compatibility of displacement as well as constitutive laws [43]. In addition, different assumptions about the variables and parameters, which affect the abovementioned mechanics principles, have influence on the definition of a specific numerical model [23],[43] and on the related final results. In addition, the perfect knowledge of a physical problem by means of engineering/mathematical models is not ever possible. Therefore, the evaluation of the partial safety factor γ_{Rd} representative of the modelling uncertainty for NLFEAs in cyclic loading conditions is necessary. For the different experimental tests [24]-[28], Subsection 3.1 comments different plausible modelling hypotheses that an engineer or practitioner may use to perform NLFEAs. Subsection 3.2 describes the global structural resistances computed numerically through NLFEAs with a comparison to the experimental results.

3.1 Epistemic uncertainties within the numerical simulations

Different modelling hypotheses can be assumed to define plane stress NLFE models of RC structures under cyclic loads. In this study, two numerical codes [44]-[45], denoted with the letters A and B in order to not advertise a specific software house, are employed to simulate the experimental results adopting four-nodes iso-parametric quadrilateral plane stress finite elements based on linear interpolant shape functions and 2x2 Gauss integration points. The definition of the FE meshes is developed after a calibration process specific for each experimental test and numerical code. The standard Newton-Raphson method [1] is applied for the numerical solution of the non-linear equations. In detail, for both numerical code A and B, the following modelling hypotheses are performed:

- for concrete in compression: non-linear behaviour with compression softening and reduction of the compressive strength due to transversal cracking are considered. Specifically, the model of [47] is herein adopted to reproduce the mono-axial concrete behaviour both in unconfined and confined conditions (where closed stirrups are provided);
- for shear behaviour of concrete: a constant value of the shear retention factor accounting for reduction of concrete shear stiffness after cracking (shear retention factor variable from a minimum value of 0.1 to a maximum value of 0.3) [46] is assumed in order to model the influence of aggregate interlock in cyclic response of the walls [48];
- smeared cracking with fixed crack direction model [46]-[51];
- tri-linear constitutive law for steel reinforcement [46] with cyclic damaging process modelled according to the approach of [50];
- with reference to the modelling of concrete cyclic response, the un-loading/re-loading path is characterized by a linear function secant to the origin both relating to compressive and tensile concrete response [48];

- discrete models of the reinforcement with the hypothesis of perfect bond without slip between concrete and embedded reinforcement [46];
- uniaxial model for concrete behaviour extended to bi-axial plane stress configuration according to [52];
- the tensile concrete strength and Young's modulus are derived from the experimental compressive strength in compliance with [36].

All the main hypotheses useful to define the plane stress NLFEAs, employing both Software A and B [44]-[45], are summarized in the Table 1. Moreover, other differentiations have been specified regarding both the concrete tensile mechanical behavior and the shear stiffness in cracked concrete.
Although concrete is known to present a quasi-brittle compressive response with a brittle tensile behavior, the interaction between reinforcement bars and concrete in cracks provides the "tension stiffening effect" [53]. To account for this effect in numerical simulations, the constitutive tensile model may be properly modified adopting a tension softening constitutive law to simulate the post peak behavior of concrete in tension. Precisely, elastic-brittle, elastic-plastic and a LTS (i.e., linear tension softening) are herein assumed as three different tension softening laws (Fig. 1) to cover the different plausible modelling hypotheses [20],[46]. The first two hypotheses are conceived as lower and upper bounds (i.e., non-physical modelling hypotheses). Whereas, the LTS law is a physical modelling hypothesis and its calibration has been developed through an iterative procedure to best fit each experimental test within the use of a specific numerical code. In this iterative procedure, the ultimate tensile deformation $\varepsilon_{\alpha,LTS}$ of concrete (Fig. 1) has been computed depending on the corresponding elastic one ε_{ct} (Fig. 1) assuming the following range of variation: from $2\varepsilon_{ct}$ to $10\varepsilon_{ct}$.

Table 1. Scheme of the modelling hypotheses used to define NLFE models.

	Numerical code A	*Numerical code B*
Equilibrium	- Standard Newton-Raphson (linear approximation hypothesis) [1] - Displacement based convergence criteria with tolerance set equal to 2% and maximum number of iterations set equal to 200 - Load step sizes adopted in compliance with the experimental loading process to achieve an appropriate accuracy of the results	
Compatibility	*Finite Elements* - Iso-parametric quadrilateral plane stress (4 nodes, 2x2 Gauss points integration scheme with linear shape functions) - Discrete reinforcement - Element size properly defined through an iterative procedure of numerical accuracy	
Constitutive laws	*CONCRETE* - Fixed smeared cracking model, constant shear retention factor β equal to: a) 0.1 b) An intermediate value chosen to best fit the experimental test c) 0.3 - Uniaxial model extended to plane stress state according to [52] - Non-linear compressive response with post peak linear softening - Tension (distinction between 3 modelling hypotheses): a) Elastic - Brittle b) LTS: Elastic with post peak linear tension softening c) Elastic - perfectly plastic - Linear un-loading/re-loading path secant to the origin both concerning compressive and tensile responses *REINFORCEMENT STEEL* - Tri-linear constitutive law with cyclic behaviuor according to *Menegotto and Pinto* [50] model	

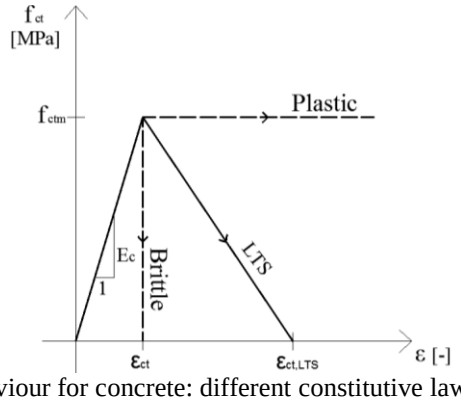

Fig.1. Tensile behaviour for concrete: different constitutive laws according to [20].

According also to [20], any dependence on the concrete properties and on the type of software is recognized.

As for the shear stiffness, the shear retention factor β is defined as the ratio between the shear stiffness of concrete after and before cracking. This parameter is extremely complex to be evaluated and may have strong implications on the results of NLFEAs related to RC members subjected to cyclic loads. Specifically, in this study, for each numerical code and tensile behaviour and experimental test, three different models are defined for the shear retention factor: for two models the extreme limit values for β (i.e., 0.1 and 0.3) are assumed, and, for a third model an iterative process is used to define the most appropriate value of β conditional to the range 0.1-0.3 [54]-[59] together with the LTS law properties to best fit each experimental test within the use of each numerical code. The selection of the shear retention factor β can be related to a physical variable, even though it may include effects of other parameters which are not considered while the resistance model is defined (i.e., epistemic uncertainty). The details about the calibration of the whole numerical models are reported in Tables A1-A5 in the Appendix concerning mesh density, LTS ultimate tensile deformation $\varepsilon_{ct,LTS}$ and shear retention factor β. Altogether, 18 different modelling hypotheses (i.e., structural models M_j with $j=1,\ldots,18$ representative of the epistemic uncertainties [20]-[32]) derive from the combination of the three different concrete tensile behaviours with the three different values of shear retention factor and the two software codes. A schematic summary of the modelling hypotheses is depicted in Figure 2. It follows that a wide study composed of 306 NLFEAs (Figure 2) can be carried out to investigate the resistance modelling uncertainties assuming the 18 different structural models for the 17 various experimental tests (discussed in the next subsection).

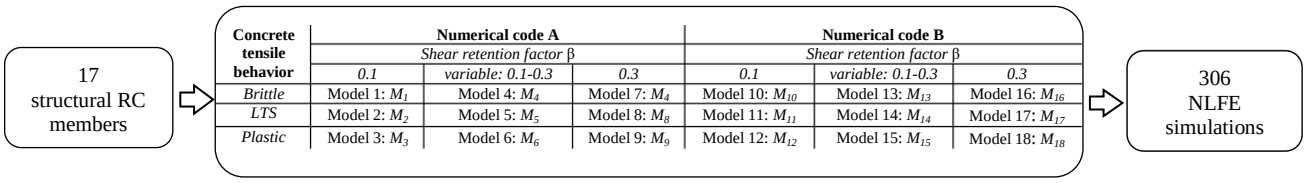

Concrete tensile behavior	Numerical code A			Numerical code B		
	Shear retention factor β			*Shear retention factor* β		
	0.1	*variable: 0.1-0.3*	*0.3*	*0.1*	*variable: 0.1-0.3*	*0.3*
Brittle	Model 1: M_1	Model 4: M_4	Model 7: M_4	Model 10: M_{10}	Model 13: M_{13}	Model 16: M_{16}
LTS	Model 2: M_2	Model 5: M_5	Model 8: M_8	Model 11: M_{11}	Model 14: M_{14}	Model 17: M_{17}
Plastic	Model 3: M_3	Model 6: M_6	Model 9: M_9	Model 12: M_{12}	Model 15: M_{15}	Model 18: M_{18}

Fig. 2. Scheme of the 18 different structural models to investigate the resistance model uncertainties.

3.2 Comparison between the NLFEA and experimental test results

This section deals with the laboratory tests examined by [24]-[28] and carried out on 17 different RC shear walls cyclically loaded up to failure in line with the specific loading processes. All the specimens, realized in laboratory, have statically determined configurations.

The numerical and experimental results, expressed in terms of lateral load vs displacement diagrams, are herein compared. It can be highlighted that the experimental tests can be affected by experimental systematic errors, regarding the geometry or the constraints, which represent another uncertainty source. However, as specified in [38],[39] and according to [20], the test uncertainty can

be neglected if the corresponding COV is equal or lower than 0.05 and the COV of model uncertainty is equal or higher than 0.10, as explained in Section 4. For each wall, the top and bottom beams are considered as stiff members and, for instance, modelled by means of linear elastic material (with Young modulus evaluated in compliance to the compressive strength presented by the experimental test reports [36]). In the following, both the numerical and experimental tests are commented in detail and the results are shown in Figures A1-A17 in the Appendix.

The laboratory experience of Pilakoutas and Elnashai [24] is represented by six RC walls designed in pairs in order to have the same percentage of bending reinforcement but different percentage of shear reinforcement. For this work, only 3 of the walls are taken into consideration denoted respectively as SW4, SW6, SW8 having the following geometrical characteristics: 1.20 m high, 0.6 m wide, 0.06 m thick and stiffened by a 0.2 m x 0.25 m inferior beam, and by a 0.2 m x 0.15 m superior beam useful to spread the applied horizontal load (Figures A1(g), A2(g) and A3(g)). All the walls are subjected to the same load history. The tests were carried out in displacement control from 2 mm up to failure, performing two complete cycles with a 2 mm increment. The compressive strength of concrete varies from 36.9 to 45.8 MPa in the different tests, whereas the flexural reinforcement remains constant in the web differently to the shear reinforcement and the vertical reinforcement that vary in the boundary elements. The numerical outcomes from the simulations expressed in terms of peak global structural resistance are presented in Tables 2 - 3. The results from NLFEAs are plotted in Figures A1-A3 (a)-(f) for the different modeling hypotheses. In general, the lowest peak lateral loads are obtained when the elastic-brittle constitutive relationship for concrete tensile behavior is adopted, while the numerical models with plastic constitutive law always overestimate both the peak load and stiffness. It can also be noted that the best results are obtained for a shear retention factor equal or close to 0.1 for the tests SW6 and SW8. All the simulations generally overestimate the global structural resistance, but underestimate the ductility because many simulations fail before if compared to the experimental results. Figure A1-A3 (a-c) and (d-f) show how the results depend on the numerical code choice (numerical code A and B, respectively): in Figures A1-A3 (a-c) the simulations fail before the end of the load history, while in Figures A1-A3 (d-f) the simulations reach the end of the analysis but overestimate the resistance, especially, for the Models 12, 15 and 18. The failure mode consists of the yielding of the main reinforcements and of the crushing of concrete in the boundary compressed element on the opposite side.

Table 2. Peak resistances from both the experimental tests $R_{EXP,i}$ [24] and NLFEAs $R_{NLFEA,i}$ for the different structural models, Numerical code A.

Ref. [*]	**Exp. test**	$R_{EXP,i}$ **[kN]**	$R_{NLFEA,i}$ **[kN]**								
			M_1	M_2	M_3	M_4	M_5	M_6	M_7	M_8	M_9
[24]	SW4	103.0	124.0	103.4	135.4	124.9	126.4	137.4	127.8	125.5	121.8
	SW6	108.6	100.1	120.8	122.2	117.6	121.3	134.3	123.0	124.5	136.0
	SW8	95.1	128.5	127.3	142.2	133.0	130.9	149.1	137.7	135.2	152.8

Table 3. Peak resistances from both the experimental tests $R_{EXP,i}$ [24] and NLFEAs $R_{NLFEA,i}$ for the different structural models, Numerical code B.

Ref. [*]	**Exp. test**	$R_{EXP,i}$ **[kN]**	$R_{NLFEA,i}$ **[kN]**								
			M_{10}	M_{11}	M_{12}	M_{13}	M_{14}	M_{15}	M_{16}	M_{17}	M_{18}
[24]	SW4	103.0	126.3	133.5	151.6	125.8	133.1	152.8	127.8	139.1	154.3
	SW6	108.6	110.3	121.3	142.9	110.8	125.4	142.7	111.6	122.7	143.7
	SW8	95.1	128.0	139.4	159.2	127.8	137.7	160.4	131.9	140.8	160.5

The laboratory tests of Lefas and Kotsovos [25] are related to four identical walls of dimensions 1300x650x65mm, that are constrained inferiorly by a beam of section 200x300mm which simulates a stiff foundation. At the top there is a stiff beam useful to uniformly transmit the imposed

displacement on the top of the wall. The flexural reinforcement is represented by ϕ8/100mm in the web, while the distance is reduced to 70mm in the boundary elements. Similarly, the shear reinforcement is composed of ϕ6.25/260mm over the entire width of the wall and of additional stirrups of ϕ4/130mm in the boundary elements. Note that only the shear walls denoted as SW31, SW32 and SW33 are herein considered (Figures A4(g), A5(g) and A6(g)). The experimental tests present a load history composed of four or five cycles with displacements of a few millimeters and then of a monotonic displacement increase up to failure. The compressive strength of concrete varies in the range 35-53 MPa in the different tests. The numerically computed peak global structural resistances are listed in Tables 4 - 5. Figures A4-A6 (a)-(f) show that the models related to elastic-plastic model for the tensile response of concrete (i.e., Models 3, 6, 9, 12, 15, 18) always overestimate both the resistance and stiffness, while models having the assumption of elastic-brittle or linear tension softening in tension have more or less the same behavior with a stiffness similar to the actual one in the cyclic phase and, in general, an underestimation of the resistance. It can be also noted that an increase of the shear retention factor increases leads to an increase of the dissipated energy. The failure mode is reached through the yielding of the tensile reinforcements and crushing of concrete located at the bottom of the boundary elements. Some simulations do not reach the ultimate experimental displacement but fail upon reaching the maximum load or for a slightly greater displacement with respect to the one achieved in the cyclic phase.

Table 4. Peak resistances from both the experimental tests $R_{EXP,i}$ [25] and NLFEAs $R_{NLFEA,i}$ for the different structural models, Numerical code A.

Ref. [*]	**Exp. test**	$R_{EXP,i}$ **[kN]**	$R_{NLFEA,i}$ **[kN]**								
			M_1	M_2	M_3	M_4	M_5	M_6	M_7	M_8	M_9
[25]	SW31	115.9	111.9	120.8	160.2	121.3	133.3	168.9	127.7	139.3	174.4
	SW32	111.0	110.3	114.8	142.8	114.9	118.3	142.7	119.1	131.1	144.3
	SW33	111.5	107.2	111.5	129.8	110.4	114.0	139.4	113.8	117.6	143.8

Table 5. Peak resistances from the both experimental tests $R_{EXP,i}$ [25] and NLFEAs $R_{NLFEA,i}$ for the different structural models, Numerical code B.

Ref. [*]	**Exp. test**	$R_{EXP,i}$ **[kN]**	$R_{NLFEA,i}$ **[kN]**								
			M_{10}	M_{11}	M_{12}	M_{13}	M_{14}	M_{15}	M_{16}	M_{17}	M_{18}
[25]	SW31	115.9	87.8	117.5	139.8	98.0	127.2	147.6	98.9	131.8	151.2
	SW32	111.0	93.7	101.6	129.4	93.9	101.9	129.5	99.4	102.2	129.7
	SW33	111.5	94.6	96.0	118.7	95.2	101.1	122.8	95.7	98.8	126.9

The experimental outcomes of Zhang and Wang [26] focused on four reinforced concrete walls and are denoted as SW7, SW8, SW9 and SRCW12. For this work, the last test has not been considered. The shear walls are 1.75 m high, 0.7 m wide and 0.1 m thick. The structural members present a full restraint at the base with a 0.5 m high and 0.4 m wide beam and loaded by an axial force at the top, that is considered evenly distributed at 0.25 m to the top surface of the wall, while the horizontal imposed displacement is applied at 1.5 m from the base of the wall. Hence, the effective height of the wall is 1.5 m. The walls SW7 and SW8 have the same reinforcement that consists of ϕ8/150mm as flexural reinforcement in the web, while the reinforcement for shear is composed of ϕ8/100mm over the total width of the walls and of hoops of ϕ6/50mm in the boundary elements. The difference is in the flexural reinforcement in the boundary elements of the walls which consists respectively of 4ϕ14 and 4ϕ12 on each side of the walls. The SW9 is more reinforced and presents 4ϕ20 on each boundary element and a greater amount of shear reinforcement if compared to the previous ones with ϕ8/75mm + ϕ6/150mm over the total width of the wall and hoops of ϕ6/75mm in the boundary elements. The walls also differ in the applied axial load: SW7 and SW9 have an axial-load ratio of 0.24 while SW8 has a greater axial-load ratio equal to 0.35. The loading histories are quite similar

and follow the same procedure: at the first time the axial load is applied with small incremental steps, after that the wall is subjected to the cyclic phase with a horizontal load which is divided in two steps: the first step consists of 10 cycles until the yielding of the flexural reinforcement; in the second step, at each cycle it is proceeded with a displacement increase equal to the half of the one recorded for the yielding. The peak global structural resistances obtained by means of the numerical simulations are presented in Tables 6 - 7. Figures A7(g), A8(g) and A9(g) illustrate the corresponding schematization of the numerical models, respectively. The NLFEAs results, plotted in Figures A7-A9 (a)-(f), show that models related to the elastic-plastic model for the concrete tensile behavior (green lines), always overestimate the stiffness. Models with the elastic-brittle assumption (blue lines) do not always bound inferiorly the range of the obtained numerical resistances. Figure A7-A9 (a-c) and (d-f) also show the influence of the numerical code (i.e., A and B) choice on the results. In fact, the curves in Figures A7-A9 (a-c) reflect the actual behavior for small displacement and reach the experimental peak load, while for bigger displacements there is a progressive reduction of both stiffness and resistance and in many cases the simulations fail before the end of the loading process (especially, for the models with elastic-plastic tensile behavior). Instead, the curves corresponding to numerical code B, in general, overestimate the structural resistance but reach the end of the loading history by reflecting appropriately the actual behavior.

Table 6. Peak resistances from both the experimental tests $R_{EXP,i}$ [26] and NLFEAs $R_{NLFEA,i}$ for the different structural models, Numerical code A.

Ref. [*]	**Exp. test**	$R_{EXP,i}$ **[kN]**	$R_{NLFEA,i}$ **[kN]**								
			M_1	M_2	M_3	M_4	M_5	M_6	M_7	M_8	M_9
[26]	SW7	201.2	189.7	195.7	206.4	203.3	202.5	209.9	212.1	206.3	224.9
	SW8	224.0	223.6	220.1	236.7	227.0	223.7	239.9	239.8	234.6	254.4
	SW9	303.5	323.6	325.0	345.0	345.7	338.1	360.4	360.4	345.3	367.4

Table 7. Peak resistances from both the experimental tests $R_{EXP,i}$ [26] and NLFEAs $R_{NLFEA,i}$ for the different structural models, Numerical code B.

Ref. [*]	**Exp. test**	$R_{EXP,i}$ **[kN]**	$R_{NLFEA,i}$ **[kN]**								
			M_{10}	M_{11}	M_{12}	M_{13}	M_{14}	M_{15}	M_{16}	M_{17}	M_{18}
[26]	SW7	201.2	226.0	223.2	241.5	240.3	236.9	255.1	252.4	249.3	264.2
	SW8	224.0	232.3	226.9	243.8	244.6	239.8	250.4	255.9	247.8	252.2
	SW9	303.5	322.7	318.1	344.4	335.1	329.2	352.3	345.1	337.4	357.4

The laboratory tests of Oesterle et al. [27] have analysed the behaviour of several anti-seismic cantilevers subjected to horizontal cyclical actions. For this study, the specimens denominated as B6, B7, B8 and F2 are considered and differ in the shape of the cross section and in the arrangement of the reinforcements. These cantilevers are 4.57 m high, with a total width of 1.91 m and a web thickness of 0.102 m, and are constrained at the base through a 0.61 m high and 1.22 m wide rigid beam and at the top by a 0.203 m high and 1.22 m wide slab. The specimens B6, B7 and B8 have the same barbell shape (rectangular shape with boundary square elements of 305x305mm), and the same amount of vertical reinforcement, while differ in amount of shear reinforcement and in the axial load. F2 differs in the shape because has two lateral I-shaped flanges (0.91x0.102m) and a greater amount of reinforcement for bending and shear. In all tests, the vertical load was applied in such a way that the resulting axial force is applied at the top of the specimens and is vertical throughout the horizontal load cycle. Figures A10(g), A11(g), A12(g) and A13(g) represent the corresponding schematization of the numerical models, respectively. Hence, an increasing displacement is imposed to the top plate providing a series of increments and each one consists of three complete cycles. In particular, three increments are applied up to the first yield, after that an additional displacement of 25 mm for each increment is imposed. The compressive strength of concrete varies between 21.8 and 49.3 MPa in the different tests, while the axial load varies in a

range of 2.93-3.76 MPa. The numerical outcomes, in terms of peak global structural resistance, are listed in Tables 8 - 9. Figures A10-A13 (a)-(f) illustrate that in general the peak horizontal load is overestimated, in particular when the elastic-plastic behavior of the concrete in tension is considered. In many simulations this overestimation can be greater than 30%. Despite of this overestimation, all the models reproduce the experimental failure mechanism that consists in the crushing of concrete in the bottom corner of the web, where the compression force is high, and the cross section is smaller with a lower degree of confinement in comparison to the boundary elements.

Table 8. Peak resistances from both the experimental tests $R_{EXP,i}$ [27] and NLFEAs $R_{NLFEA,i}$ for the different structural models, Numerical code A.

Ref. [*]	**Exp. test**	$R_{EXP,i}$ **[kN]**	$R_{NLFEA,i}$ **[kN]**								
			M_1	M_2	M_3	M_4	M_5	M_6	M_7	M_8	M_9
[27]	B6	854.7	886.9	843.9	984.0	925.7	850.1	968.0	938.9	878.0	974.4
	B7	1012.8	1051.0	1012.0	1279.0	1110.0	1051.0	1298.0	1122.0	1069.0	1337.0
	B8	1063.7	1123.0	1092.0	1250.0	1199.0	1167.0	1309.0	1236.0	1172.0	1341.0
	F2	923.8	860.3	920.2	1158.0	917.2	918.2	1201.0	951.6	995.7	1217.0

Table 9. Peak resistances from both the experimental tests $R_{EXP,i}$ [27] and NLFEAs $R_{NLFEA,i}$ for the different structural models, Numerical code B.

Ref. [*]	**Exp. test**	$R_{EXP,i}$ **[kN]**	$R_{NLFEA,i}$ **[kN]**								
			M_{10}	M_{11}	M_{12}	M_{13}	M_{14}	M_{15}	M_{16}	M_{17}	M_{18}
[27]	B6	854.7	904.8	920.9	1046.4	907.8	933.4	1040.1	935.2	942.9	1041.7
	B7	1012.8	1290.3	1256.6	1458.1	1321.8	1276.9	1470.6	1349.1	1288.6	1486.2
	B8	1063.7	1336.4	1303.4	1472.4	1387.8	1303.1	1456.9	1394.2	1304.7	1458.8
	F2	923.8	1153.4	1130.0	1374.2	1154.2	1125.5	1383.0	1214.9	1126.8	1389.4

Finally, the experience concerning the laboratory tests of [28], that investigated the response of RC walls subjected to a quasi-static cyclic action, is considered. Specifically, four specimens (WSH2, WSH3, WSH4 and WSH6) are herein considered and numerically reproduced. The walls have identical geometry (i.e., 4.03 m high, 2 m wide and 0.15 m thick) and are fixed at the base through a beam integral with the supporting surface of section 0.6 m high and 0.7 wide and protruding 0.4 m from the two sides of the wall, while at the top there is a 0.4 m thick and 0.92 m high beam with a taper to favourite the connection with the wall. On this upper beam the axial load is adequately provided and the cyclic loading history is applied by means of actuators located at a distance of 0.39 m from the upper edge. The walls are all reinforced with ϕ6/150 mm located horizontally along the entire width of the wall. They differ from each other in the percentage of flexural reinforcement and in the percentage of shear reinforcement in the boundary element as well as for the value of the applied axial load. The WSH2 wall has flexural reinforcements of 6ϕ10, spaced at 75 mm in the boundary elements, and of 24ϕ6 in the web spaced at 125 mm (symmetrically starting from the outside to the center). The shear reinforcement consists of ϕ6/150 mm across the entire width, as mentioned above, and of stirrups ϕ6/75mm that enclose the ϕ10s and of a ϕ4.2 hoop that binds the two central ϕ10s. The specimen WSH3 is reinforced with 6ϕ12 on the boundary elements spaced at 100 mm, and with 22ϕ8 in the web spaced at 125 mm, and has a shear reinforcement identical to the WSH2. The wall WSH4 differs from the WSH3 concerning the shear reinforcement composed of ϕ6/150 mm across the entire width and of ϕ6/150 mm in the boundary element. The specimenWSH6, on the other hand, has the same bending reinforcement of the previous one, but a higher reinforcement percentage in the boundary element. There are ϕ6/50 mm closed stirrups around the four lateral flexural bars, and another closed stirrup of 4.2/50 mm which encloses the four inners ϕ12. The compressive strength of concrete and axial load are similar for WSH2, WSH3

and WSH4 with values of 40.5, 39.2 and 40.9 MPa and 691, 686 and 695 kN, respectively. While WSH6 has a higher compressive strength equal to 45.6 MPa and an axial load of 1476 kN. The loading history is in line with the standard protocol by Park [60]: firstly, the axial load is applied to the wall and it is maintained constant during all the testing procedure; secondly, the incremental cyclic horizontal imposed displacement has been applied through the hydraulic actuators. During the experiments, the nominal yield displacement has been determined after the first cycles. Then, the magnitude of the successive displacement cycles has been incremented of the same magnitude of the nominal yield displacement by until the failure occurred. At each displacement level the wall has been subjected to two full cycles. The schemes representing the numerical models are reported in Figures A14(g)-A17(g). The results of numerical simulations expressed as peak global structural resistance are presented in Tables 10 - 11. Figures A14-A17 (a)-(f) illustrate that models that assume the tensile behaviour of the concrete brittle or LTS reproduce efficiently the actual behaviour, while the models with concrete tensile behaviour perfectly plastic overestimate both the resistance and stiffness.

Table 10. Peak resistances from both the experimental tests $R_{EXP,i}$ [28] and NLFEAs $R_{NLFEA,i}$ for the different structural models, Numerical code A.

Ref. [*]	**Exp. test**	$\boldsymbol{R_{EXP,i}}$ **[MPa]**	$\boldsymbol{R_{NLFEA,i}}$ **[MPa]**								
			M_1	M_2	M_3	M_4	M_5	M_6	M_7	M_8	M_9
[28]	WSH2	359.0	378.3	363.2	512.0	386.0	369.4	521.6	436.6	407.5	562.5
	WSH3	454.0	441.4	443.6	604.8	454.0	448.9	659.5	549.1	474.3	674.2
	WSH4	443.0	450.8	448.9	508.5	467.6	450.7	525.9	484.2	523.8	567.7
	WSH6	597.0	633.9	624.4	732.7	665.2	658.3	744.8	689.0	678.2	794.9

Table 11. Peak resistances from both the experimental tests $R_{EXP,i}$ [28] and NLFEAs $R_{NLFEA,i}$ for the different structural models, Numerical code B.

Ref. [*]	**Exp. test**	$\boldsymbol{R_{EXP,i}}$ **[MPa]**	$\boldsymbol{R_{NLFEA,i}}$ **[MPa]**								
			M_{10}	M_{11}	M_{12}	M_{13}	M_{14}	M_{15}	M_{16}	M_{17}	M_{18}
[28]	WSH2	359.0	376.9	410.1	493.8	367.7	413.7	489.9	389.6	410.3	488.6
	WSH3	454.0	481.6	532.7	603.6	500.1	542.2	617.0	483.1	532.4	607.3
	WSH4	443.0	404.8	441.5	474.4	423.3	442.1	481.0	435.5	457.8	483.5
	WSH6	597.0	617.7	661.6	739.5	624.8	664.4	758.2	638.6	673.4	768.9

The outcomes deriving from the mentioned above 306 non-linear FE simulations highlight the influence of the different modelling hypotheses since the geometry, the materials and the loading process are numerically reproduced in line with each experimental test. The numerical results are herein adopted to evaluate the resistance modelling uncertainty in plane stress NLFEAs of RC members subjected to cyclic loads.

4. CALIBRATION OF THE RESISTANCE MODEL UNCERTAINTY PARTIAL SAFETY FACTOR

The present section is composed of four sub-sections aimed at assessing the partial safety factor related to the uncertainty in the definition of the resistance model through NLFEAs with cyclic loading processes for design or verification aims. Sections 4.1 and 4.2 describe the statistical and probabilistic processing of the results from numerical simulations in comparison to the experimental ones, whereas Sections 4.3 and 4.4 discuss the evaluation of the resistance model uncertainty partial safety factor for RC structures under cyclic loads.

4.1 Evaluation of the epistemic uncertainty in the definition of the resistance model

In compliance with Section 2, the resistance modelling uncertainty ϑ can be determined considering the experimental and NLFEA results. According to Eq.(2), in the tests considered for the present investigation, the vector of the variables X is represented by the set of assumptions performed to define the mechanical properties of materials concerning each modelling hypothesis, while the vector of the variables Y is reflected by the parameters and aspects that are not accounted for by the specific structural model. Specifically, for example, the influence on the structural response of the bond between reinforcement and concrete as well as the presence of a certain degree of confinement in the central region of the walls have not been included in the numerical models. However, their contribution to the global structural response is hidden within the results of the experimental investigations and is indirectly included in the definition of the resistance model uncertainty random variable ϑ by means of the information of Y. The ratios ϑ_i (with $i=1,...,17$) computed for all the walls described in Section 3 and conditional to each specific structural model (i.e., modelling hypotheses – Models 1-18) are presented in Table 12.

As also previously underlined and according to [20], the outcomes in Table 12 demonstrate that the two extreme hypotheses regarding concrete tensile behaviour (i.e., elastic-brittle and elastic-plastic) do not necessarily represent the bound limits concerning the experimental peak load. Moreover, they highlight the effectiveness of the different assumptions to reproduce the cyclic response of the structural members. In fact, the differences between the experimental and the numerically predicted peak loads may be significantly high: unsafe values of ϑ up to 0.59 are obtained for the shear walls of [24]. It means that the finite element models are not always able to reproduce the experimental behaviour accurately but sometimes overestimate the peak resistances of the walls under specific hypotheses leading to unsafe estimations. This issue is a crucial aspect in relation to safety verifications for seismic analyses. It follows that it is crucial to calibrate and propose an appropriate value for the resistance modelling uncertainty partial safety factor for NLFEAs of RC systems.

Table 12. $\vartheta_i = R_{EXP,i}/R_{NLFEA,i}$ for all the sets of modelling hypotheses.

Ref [*]	Exp. tests	Structural model																	
		1	2	3	4	5	6	7	8	9	10	11	12	13	14	15	16	17	18
[24]	SW4	0.83	1.00	0.76	0.82	0.81	0.75	0.81	0.82	0.85	0.82	0.77	0.68	0.82	0.77	0.67	0.81	0.74	0.67
	SW6	1.08	0.90	0.89	0.92	0.90	0.81	0.88	0.87	0.80	0.98	0.90	0.76	0.98	0.87	0.76	0.97	0.88	0.76
	SW8	0.74	0.75	0.67	0.72	0.73	0.64	0.69	0.70	0.62	0.74	0.68	0.60	0.74	0.69	0.59	0.72	0.68	0.59
[25]	SW31	1.04	0.96	0.72	0.96	0.87	0.69	0.91	0.83	0.66	1.32	0.99	0.83	1.18	0.91	0.79	1.17	0.88	0.77
	SW32	1.01	0.97	0.78	0.97	0.94	0.78	0.93	0.85	0.77	1.18	1.09	0.86	1.18	1.09	0.86	1.12	1.09	0.86
	SW33	1.04	1.00	0.86	1.01	0.98	0.80	0.98	0.95	0.78	1.18	1.16	0.94	1.17	1.10	0.91	1.16	1.13	0.88
[26]	SW7	1.06	1.03	0.97	0.99	0.99	0.96	0.95	0.98	0.89	0.89	0.90	0.83	0.84	0.85	0.79	0.80	0.81	0.76
	SW8	1.00	1.02	0.95	0.99	1.00	0.93	0.93	0.95	0.88	0.96	0.99	0.92	0.92	0.93	0.89	0.88	0.90	0.89
	SW9	0.94	0.93	0.88	0.88	0.90	0.84	0.84	0.88	0.83	0.94	0.95	0.88	0.91	0.92	0.86	0.88	0.90	0.85
[27]	B6	0.96	1.01	0.87	0.92	1.01	0.88	0.91	0.97	0.88	0.94	0.93	0.82	0.94	0.92	0.82	0.91	0.91	0.82
	B7	0.96	1.00	0.79	0.91	0.96	0.78	0.90	0.95	0.76	0.78	0.81	0.69	0.77	0.79	0.69	0.75	0.79	0.68
	B8	0.95	0.97	0.85	0.89	0.91	0.81	0.86	0.91	0.79	0.80	0.82	0.72	0.77	0.82	0.73	0.76	0.82	0.73
	F2	1.07	1.00	0.80	1.01	1.01	0.77	0.97	0.93	0.76	0.80	0.82	0.67	0.80	0.82	0.67	0.76	0.82	0.66
[28]	WSH2	0.95	0.99	0.70	0.93	0.97	0.69	0.82	0.88	0.64	0.95	0.88	0.73	0.98	0.87	0.73	0.92	0.87	0.73
	WSH3	1.03	1.02	0.75	1.00	1.01	0.69	0.83	0.96	0.67	0.94	0.85	0.75	0.91	0.84	0.74	0.94	0.85	0.75
	WSH4	0.98	0.99	0.87	0.95	0.98	0.84	0.91	0.85	0.78	1.09	1.00	0.93	1.05	1.00	0.92	1.02	0.97	0.92
	WSH6	0.94	0.96	0.81	0.90	0.91	0.80	0.87	0.88	0.75	0.97	0.90	0.81	0.96	0.90	0.79	0.93	0.89	0.78

4.2 Statistical analysis of the results and definition of the probabilistic models

This section presents the probability density functions (PDFs) used to represent the resistance modelling uncertainty random variable. Graphical analyses of the ratios $\vartheta_i = R_{EXP,i}/R_{NLFEA,i}$ related to the Models 3 and 11, for example, are shown in Figures 3 and 4 through the frequency histogram (Figures 3-4(a)) and sample vs theoretical probability plot (Figures 3-4(b)) confirming the use of the lognormal probabilistic distribution. Analogous results are obtained for the other sets of modelling hypotheses, which compose the set of the prior information as commented in the next subsections. This result is in agreement with [21]. In addition, the Chi-square, Anderson-Darling tests have also confirmed, for each structural model (i.e., Models 1-18), the possibility to adopt lognormal probabilistic distributions with 5% significance levels. Contextually, the same statistical tests and the graphical analyses of the random variable ϑ_i have been performed for the totality of the models, confirming the possibility to adopt a log-normal distribution (Figure 5).
Then, the same statistical tests and the graphical analyses of the ratios ϑ_i have also been performed regarding the updating (or new) information distributions, confirming the choice to adopt a log-normal distribution for each model. For example, Figures 6-7(a) and Figures 6-7(b) show, respectively, the corresponding frequency histogram and the probability plot of the updating information with respect to the Models 3 and 11, respectively. The updating distribution for the structural model M_j ($j=1,...,18$) is determined taking into account all the results with the exclusion of the ones of the model M_j itself. In other words, for the Model 3, the updating information is composed of the other different seventeen models as well as for the Model 11.

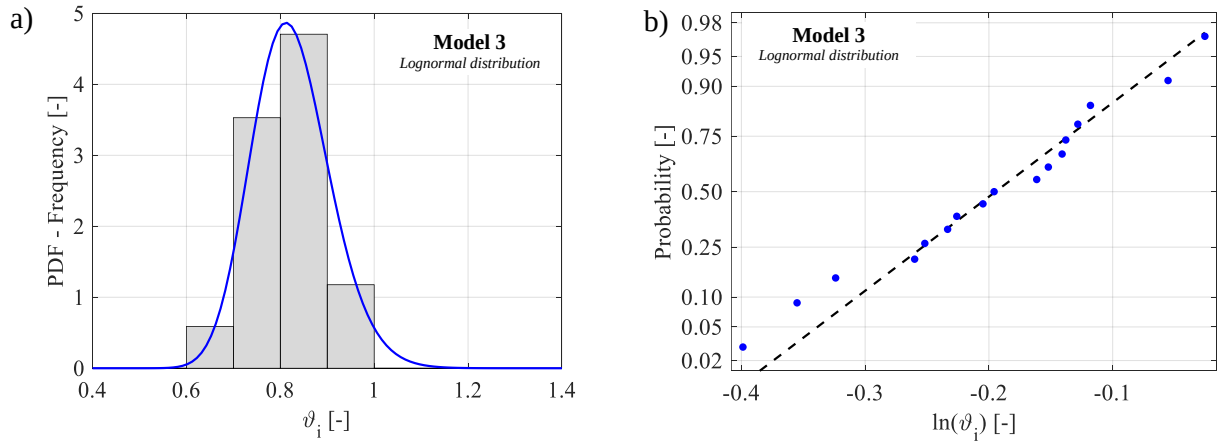

Fig. 3. Histogram and lognormal PDF of the ratio ϑ_i for the Model 3 (a); Probability plot of ln(ϑ_i) for the Model 3 (b).

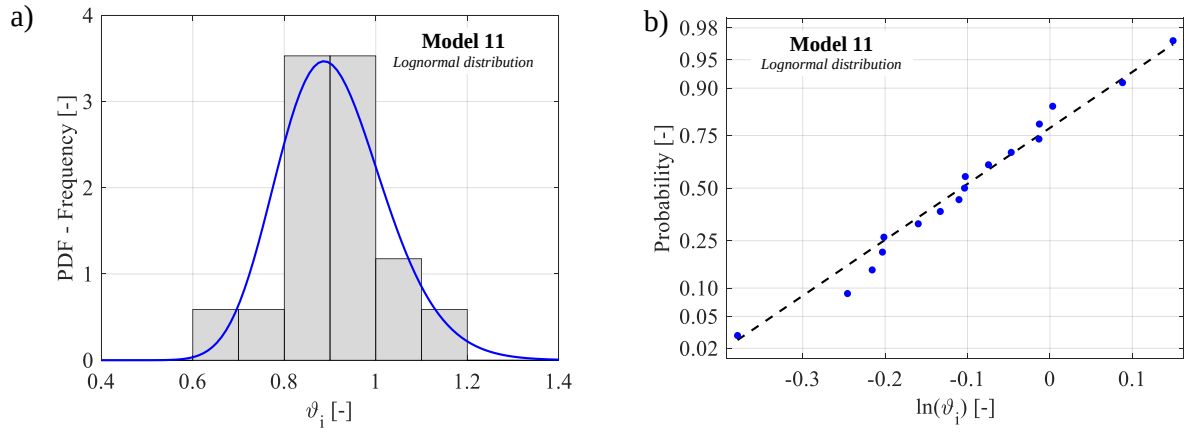

Fig. 4. Histogram and lognormal PDF of the ratio ϑ_i for the Model 11 (a); Probability plot of

$\ln(\vartheta_i)$ for the Model 11 (b).

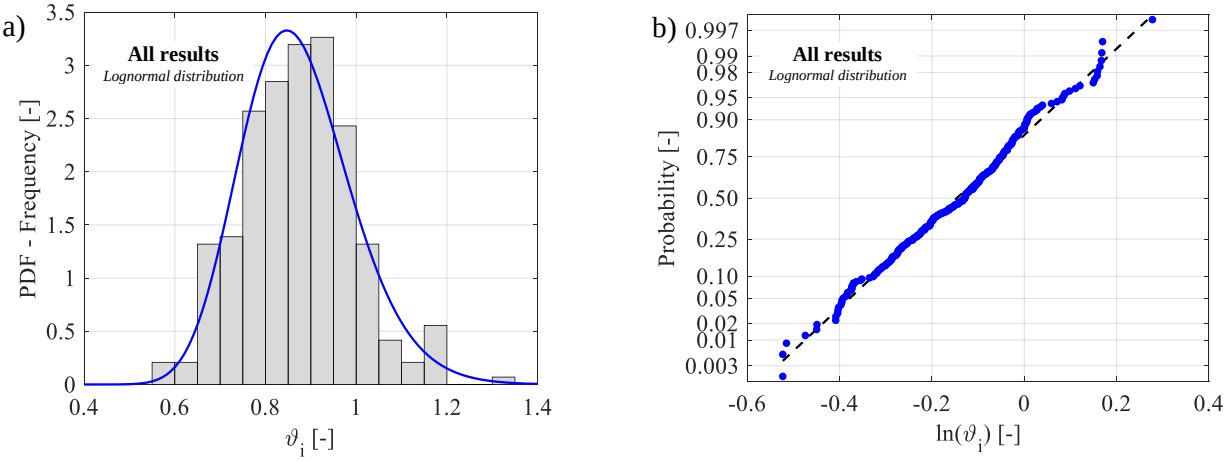

Fig. 5. Histogram and lognormal PDF of the ratio ϑ_i for all the models (a); Probability plot of $\ln(\vartheta_i)$ for all the models (b).

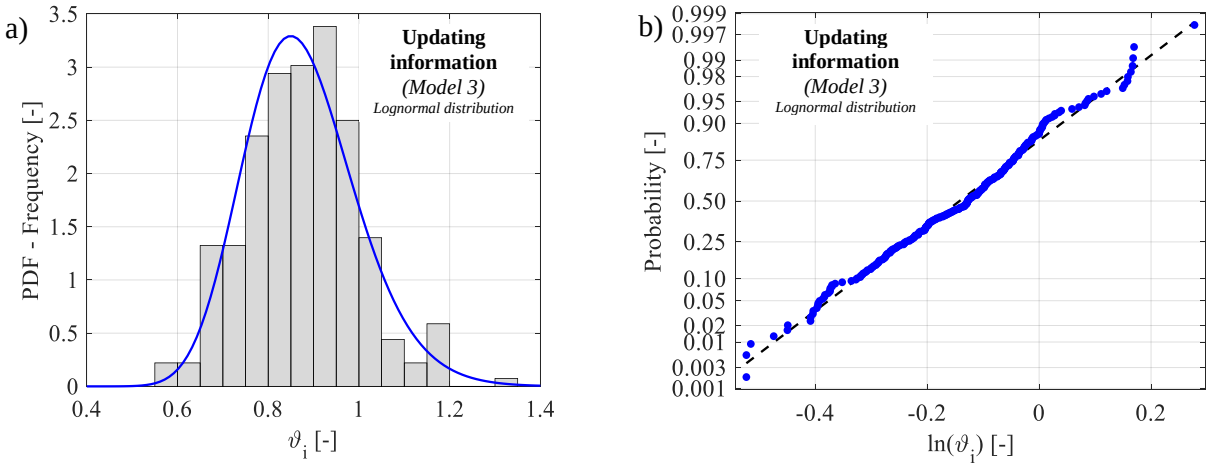

Fig. 6. Histogram and lognormal PDF of the ratio ϑ_i for the updating information with respect to Model 3 (a); Probability plot of $\ln(\vartheta_i)$ for the updating information with respect to the Model 3 (b).

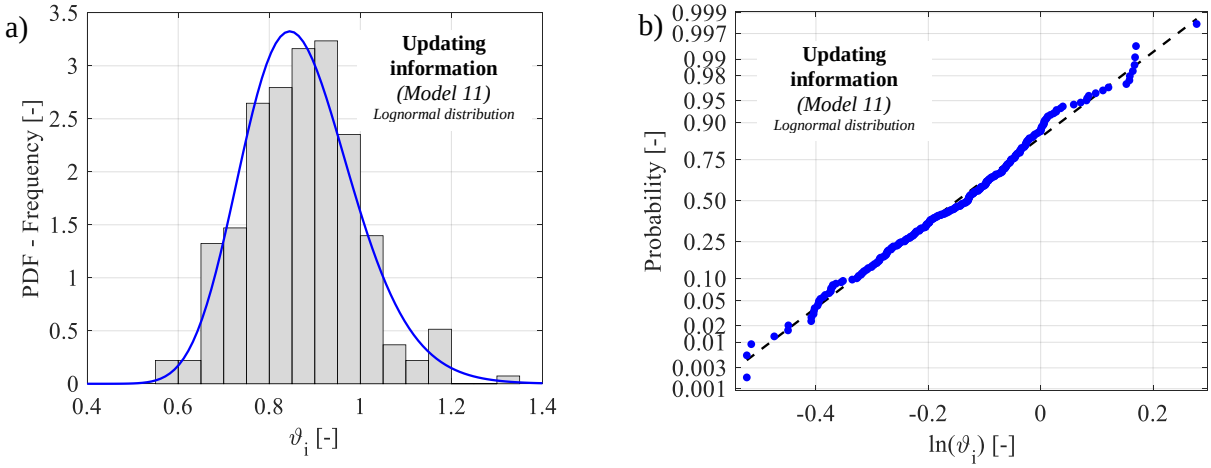

Fig. 7. Histogram and lognormal PDF of the ratio ϑ_i for the updating information with respect to Model 11 (a); Probability plot of $\ln(\vartheta_i)$ for the updating information with respect to the Model 11 (b).

4.3 Probabilistic processing of the resistance model uncertainty

With purpose to define a comprehensive probabilistic characterization of the random variable associated to the resistance modelling uncertainty due to the different modelling hypotheses, the

Bayesian approach [61] can be adopted according to the methodology defined by [20]. In particular, the 18 lognormal probability density or cumulative distribution functions (PDFs-CDFs) conditional to the adoption of a specific set of the modelling hypotheses (i.e., structural model M_j), denoted as $f(\vartheta \mid M_j)$ or $F(\vartheta \mid M_j)$ with $j=1,2,\ldots,18$, represent the prior information. All the 18 sets of modelling hypotheses are herein assumed as equiprobable. In line with [20], concerning each one of the 18 structural models M_j, the updating information is composed of the numerical results which derive from all the other 17, as summarized in Table 2. Then, the 18 updating lognormal probability density or cumulative functions $f_{Mj}(\vartheta \mid z_j)$ or $F_{Mj}(\vartheta \mid z_j)$ can be defined, for the single structural model Mj, considering the average statistical parameters (grouped in the vector z_j) of the probabilistic distributions of the other 17 structural models. The Bayesian updating allows to define the 18 posterior lognormal probability density or cumulative functions $f(\vartheta \mid M_j, z_j)$ or $F(\vartheta \mid M_j, z_j)$ conditional to each structural model M_j. Finally, defining Z as the vector which collects the average statistical parameters (i.e., μ_ϑ mean value and σ_ϑ standard deviation) concerning the 18 model-conditional posterior distributions, the average lognormal posterior PDF $f(\vartheta \mid Z)$ or CDF $F(\vartheta \mid Z)$ can be assessed and adopted to represent the resistance modelling uncertainty random variable ϑ [20].

Table 13. Statistical parameters of the prior, posterior and updating information distribution functions with the related statistical uncertainty.

Structural Model	*Prior distributions (Lognormal)* $F(\vartheta \mid M_j)$		*Statistical uncertainty*		*Updating information (Lognormal)* $F_{Mj}(\vartheta \mid z_j)$		*Statistical uncertainty*		*Posterior distributions (Lognormal)* $F(\vartheta \mid M_j, z_j)$		*Statistical uncertainty*	
	μ_ϑ [-]	V_ϑ [-]	*C(1,1)*	*C(2,2)*	μ_ϑ [-]	V_ϑ [-]	*C(1,1)*	*C(2,2)*	μ_ϑ [-]	V_ϑ [-]	*C(1,1)*	*C(2,2)*
1	0.98	0.08	4.2E-04	2.3E-04	0.87	0.14	6.3E-05	3.1E-05	0.93	0.13	1.6E-04	5.7E-06
2	0.97	0.07	3.1E-04	1.7E-04	0.87	0.14	6.3E-05	3.2E-05	0.92	0.12	1.5E-04	4.8E-06
3	0.82	0.10	5.9E-04	3.3E-04	0.88	0.14	6.4E-05	3.2E-05	0.85	0.12	1.5E-04	5.1E-06
4	0.93	0.07	3.2E-04	1.8E-04	0.88	0.14	6.5E-05	3.3E-05	0.90	0.12	1.3E-04	3.8E-06
5	0.94	0.08	3.8E-04	2.1E-04	0.88	0.14	6.5E-05	3.2E-05	0.91	0.12	1.4E-04	4.2E-06
6	0.80	0.10	6.0E-04	3.3E-04	0.88	0.14	6.3E-05	3.2E-05	0.84	0.13	1.7E-04	5.9E-06
7	0.89	0.07	2.9E-04	1.6E-04	0.88	0.14	6.6E-05	3.3E-05	0.88	0.11	1.2E-04	3.1E-06
8	0.90	0.07	2.9E-04	1.6E-04	0.88	0.14	6.6E-05	3.3E-05	0.89	0.11	1.2E-04	3.1E-06
9	0.78	0.10	5.9E-04	3.2E-04	0.89	0.13	6.2E-05	3.1E-05	0.83	0.13	1.8E-04	6.9E-06
10	0.96	0.16	1.5E-03	8.2E-04	0.87	0.13	6.0E-05	3.0E-05	0.92	0.15	2.4E-04	1.2E-05
11	0.91	0.13	9.7E-04	5.3E-04	0.88	0.14	6.3E-05	3.2E-05	0.89	0.13	1.8E-04	6.8E-06
12	0.79	0.13	9.6E-04	5.3E-04	0.88	0.13	6.1E-05	3.1E-05	0.84	0.14	2.0E-04	8.8E-06
13	0.94	0.15	1.3E-03	7.2E-04	0.88	0.13	6.2E-05	3.1E-05	0.91	0.15	2.1E-04	9.7E-06
14	0.89	0.12	8.0E-04	4.4E-04	0.88	0.14	6.4E-05	3.2E-05	0.88	0.13	1.6E-04	5.6E-06
15	0.78	0.12	8.5E-04	4.7E-04	0.89	0.13	6.1E-05	3.1E-05	0.83	0.14	2.0E-04	8.8E-06
16	0.91	0.15	1.4E-03	7.5E-04	0.88	0.13	6.2E-05	3.1E-05	0.90	0.14	2.1E-04	9.4E-06
17	0.88	0.12	8.9E-04	4.9E-04	0.88	0.14	6.4E-05	3.2E-05	0.88	0.13	1.7E-04	6.0E-06
18	0.77	0.12	8.0E-04	4.4E-04	0.89	0.13	6.1E-05	3.0E-05	0.83	0.14	2.1E-04	8.9E-06

Average statistical parameters	*Posterior distribution (Lognormal)* $F(\vartheta \mid Z)$	
	μ_ϑ [-]	V_ϑ [-]
	0.88	0.13

In Table 13, the prior, updating and posterior statistical parameters of the related probabilistic distributions are reported. The maximum likelihood criterion has been followed to estimate the statistical parameters of the prior and updating information. By evaluating the inverse of the Fischer

information matrices **C** [62], the variance of the statistical parameters μ_ϑ (i.e., C(1,1)) and σ_ϑ (i.e., C(2,2), respectively, are also reported. The posterior probabilistic distributions, representing the resistance model uncertainty for each structural model M_j, have COVs which are not negligible and vary in the range 0.12 - 0.16 (Table 13). The mean μ_ϑ values of the posterior probabilistic distributions of the structural models which present plastic response in tension for concrete are slightly higher if compared to the related prior values. This is the result of the influence of the updating distributions $F_{Mj}(\vartheta \mid z)$. In fact, the prior distributions have presented, in general, mean values μ_ϑ which correspond to a relevant unsafe bias for structural models 3,6,9,12,15,18. On the contrary, the mean values associated to the posterior probabilistic distributions of structural models 1,4,7,10,13,16 presenting a brittle behavior for concrete in tension are lower than the corresponding ones of the prior probabilistic distributions with higher coefficient of variations (especially, for the results obtained with software A).

In Figures 8(a) and 8(b) the prior, updating and posterior probabilistic distributions (i.e., PDFs-CDFs) are reported and compared. The average posterior mean value μ_ϑ and the coefficient of variation V_ϑ of the resistance modelling uncertainty related to plane stress NLFEAs of RC members subjected to cyclic loading are, respectively, equal to 0.88 and 0.13 (Table 13). As previously introduced, according to [20],[38],[39] the experimental uncertainty can be neglected as the COV V_ϑ of the resistance modelling uncertainties turns out to be higher than the value of 0.10.

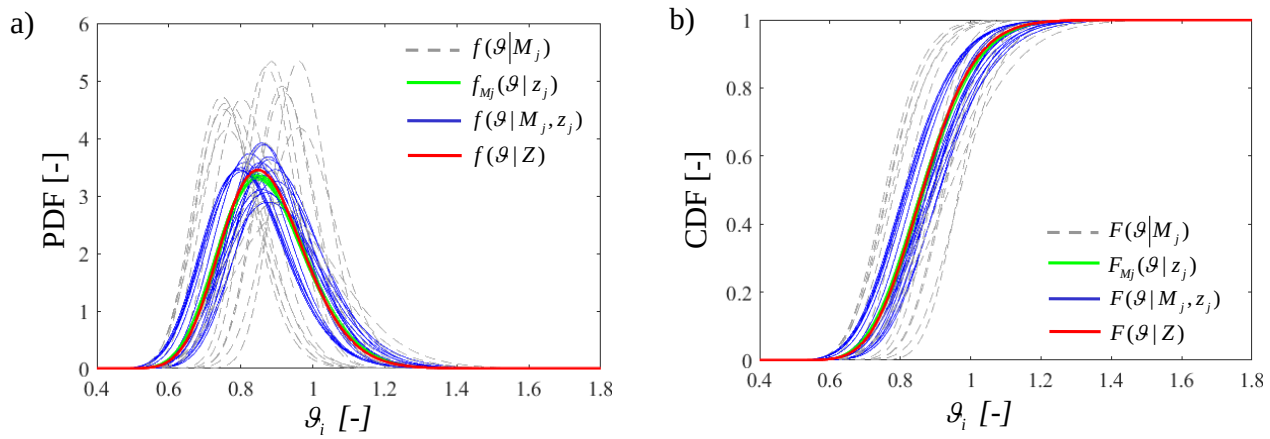

Fig. 8. Probabilistic distributions related to prior, posterior and updating information PDFs (a) and CDFs (b).

4.4 Evaluation of the resistance model uncertainty partial safety factor

In the present sub-section, the resistance model uncertainty partial safety factor γ_{Rd} for plane stress NLFEAs of RC structures subjected to cyclic loads is proposed. The values of γ_{Rd} are reported depending on the target reliability indices β proposed by design Codes and literature concerning both existing and new structures [5],[7],[14],[64]. In compliance to [5],[7],[14], the reliability level differentiation depends mainly on the consequences of structural failure, human safety and reference service life.

In line with the assumption of lognormal probabilistic distributions for the resistance model uncertainty ϑ and according to Table 13 (i.e., using μ_ϑ =0.88, V_ϑ =0.13), the partial safety factor γ_{Rd} can be evaluated through Eq.(3) adopting different target reliability indices [5] (Tables 14 - 15). Specifically, the values of γ_{Rd} reported in Table 14 are computed considering the resistance modelling uncertainty as a non-dominant resistance variable [5],[14] with the value of 0.32 for the FORM sensitivity factor α_R [20]. The non-dominant hypothesis is justified by the COV equal to V_ϑ =0.13 (Table 13) that is lower than the COV value associated to the compressive strength of concrete set equal to 0.15 [5]. It follows that the overall uncertainty of the global resistance is dominated by the material and geometry aleatory uncertainties. In this way, for new structural

systems with moderate consequences due to a structural failure and a 50 years lifetime and β=3.8, a value of 1.33 is proposed as γ_{Rd}. For existing structural systems, γ_{Rd} is variable between 1.30 to 1.48.

Table 14. Partial safety factors γ_{Rd} for plane stress NLFEAs of RC structures subjected to cyclic loads in the hypothesis of non-dominant resistance variable depending on the target reliability level [5].

	Service life	**Consequences of failure**	**Reliability index β**	**FORM factor α_R**	**Partial safety factor γ_{Rd}**
New structures	[Years]	[-]	[-]	[-]	[-]
	50	Low	3.1	Non-dominant 0.32	*1.30*
	50	Moderate	3.8		*1.33*
	50	High	4.3		*1.36*
	Residual service life		**Reliability index β**	**FORM factor α_R**	**Partial safety factor γ_{Rd}**
Existing structures	[Years]		[-]	[-]	[-]
	50		3.1 - 3.8	Non-dominant 0.32	*1.30-1.33*
	15		3.4 - 4.1		*1.31-1.35*
	1		4.1 - 4.7		*1.35-1.38*

Table 15. Partial safety factors γ_{Rd} for plane stress NLFEAs of RC structures subjected to cyclic loads in the hypothesis of dominant resistance variable depending on the target reliability level [5].

	Service life	**Consequences of failure**	**Reliability index β**	**FORM factor α_R**	**Partial safety factor γ_{Rd}**
New structures	[Years]	[-]	[-]	[-]	[-]
	50	Low	3.1	Dominant 0.8	*1.57*
	50	Moderate	3.8		*1.69*
	50	High	4.3		*1.78*
	Residual service life		**Reliability index β**	**FORM factor α_R**	**Partial safety factor γ_{Rd}**
Existing structures	[Years]		[-]	[-]	[-]
	50		3.1 - 3.8	Dominant 0.8	*1.57-1.69*
	15		3.4 - 4.1		*1.62-1.74*
	1		4.1 - 4.7		*1.74-1.85*

Table 15 reports the values of $\gamma_{Rd,}$ when the model uncertainties are dominant in comparison to the aleatory uncertainties (i.e., α_R=0.8) leading to (20%) higher values for both new and existing structural systems. Note that in this hypothesis, the partial factors corresponding to the aleatory uncertainties on material strengths (i.e., γ_c and γ_s) will be significantly decreased.

5. CONCLUSIONS

This study proposes and evaluates the values of the partial safety factor corresponding to the resistance model uncertainties (i.e., epistemic uncertainties) for 2D NLFE simulations of RC structural systems subjected to cyclic loads for seismic analyses. Various experimental tests concerning different walls subjected to cyclic shear actions have been numerically simulated through 306 NLFEAs adopting two different software codes, three different constitutive laws for

the concrete tensile behaviour and three different shear retention factors to take into account the reduction of the shear stiffness after cracking. The numerical results compared to the experimental outcomes have highlighted some differences regarding both the cyclic response and peak load. In general, it can be observed that a perfectly plastic tensile behaviour of the concrete always gives a greater overestimation of the structural resistance, and that the variation of the shear retention factor varies the amplitude of the cycle, and therefore the dissipated energy. However, in terms of resistance within a global force-based approach, for many cases, a shear retention factor close to 0.1 is the one that best fits the experimental test.
Adopting a lognormal probabilistic distribution to represent the resistance model uncertainties, the related mean and of the COV values are equal to 0.88 and 0.13, respectively. Then, following a probabilistic processing with a Bayesian updating, the partial safety factors have been calibrated in relation to both existing and new structures with the hypothesis of resistance model uncertainties as dominant or non-dominant variables with respect to the aleatory uncertainties. Finally, when the model uncertainties are non-dominant, for both existing and new ordinary structural systems characterized by moderate consequences of structural collapse and a 50 years lifetime, the resistance model uncertainty partial safety factor equal to 1.35 is suggested as a safe assumption. This proposal is necessary to cover the epistemic uncertainties to perform 2D numerical simulations of RC structures subjected to cyclic loads for design or verification aims within the seismic field.

ACKNOWLEDGEMENTS

This work is part of the collaborative activity developed by the authors within the framework of the Commission 3 – Task Group 3.1: *"Reliability and safety evaluation: full-probabilistic and semi-probabilistic methods for existing structures"* of the International Federation for Structural Concrete (*fib*).

This work is also part of the collaborative activity developed by the authors within the framework of the WP 11 – Task 11.4 – ReLUIS.

Appendix

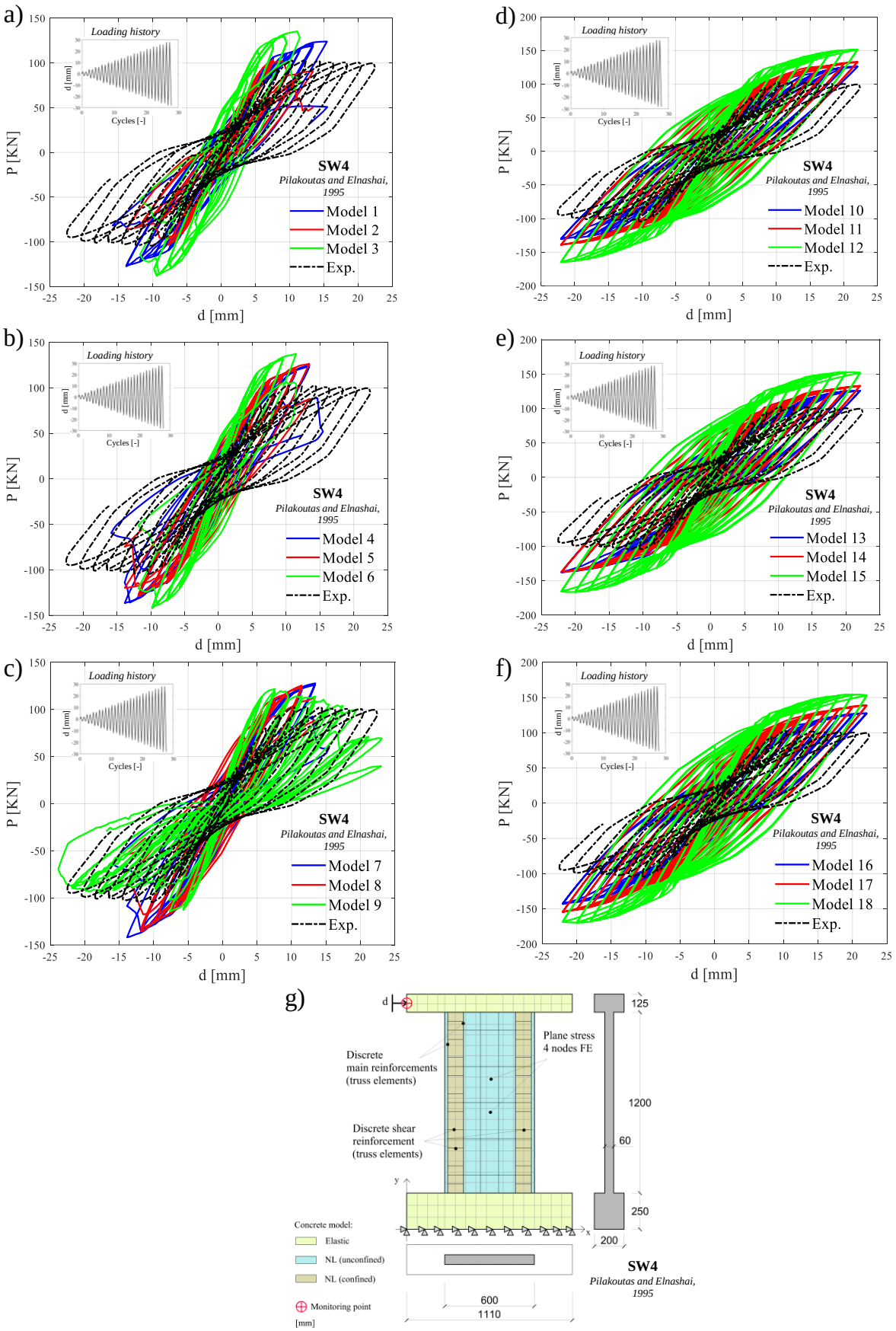

Fig. A1. Results from NLFEAs and experimental tests expressed as load vs displacement curves - SW4 of [24]; (a-c) Numerical code A, (d-f) Numerical code B. Schematization of the NLFE model (dimensions in [mm]) (g).

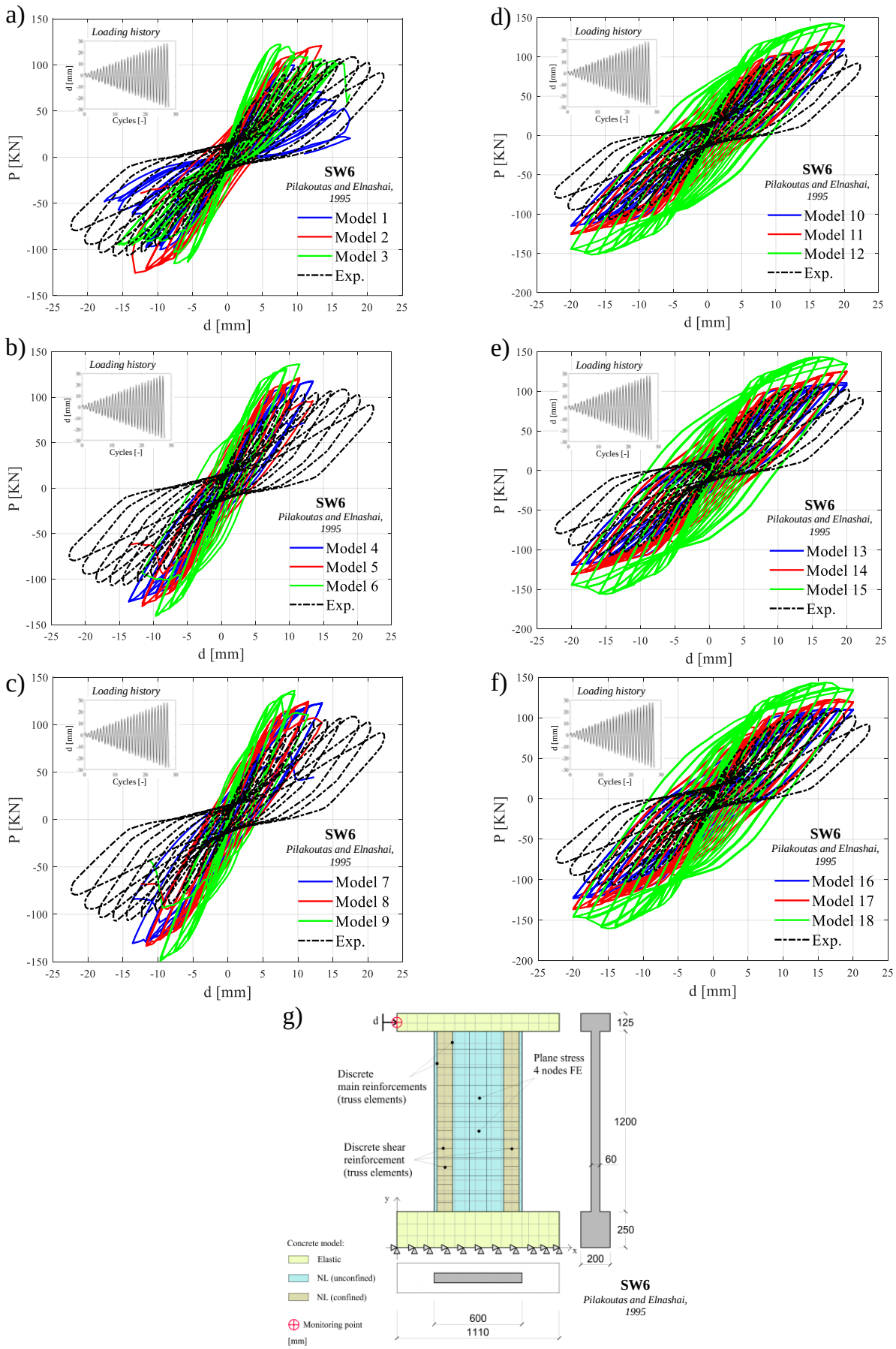

Fig. A2. Results from NLFEAs and experimental tests expressed as load vs displacement curves - SW6 of [24]; (a-c) Numerical code A, (d-f) Numerical code B. Schematization of the NLFE model (dimensions in [mm]) (g).

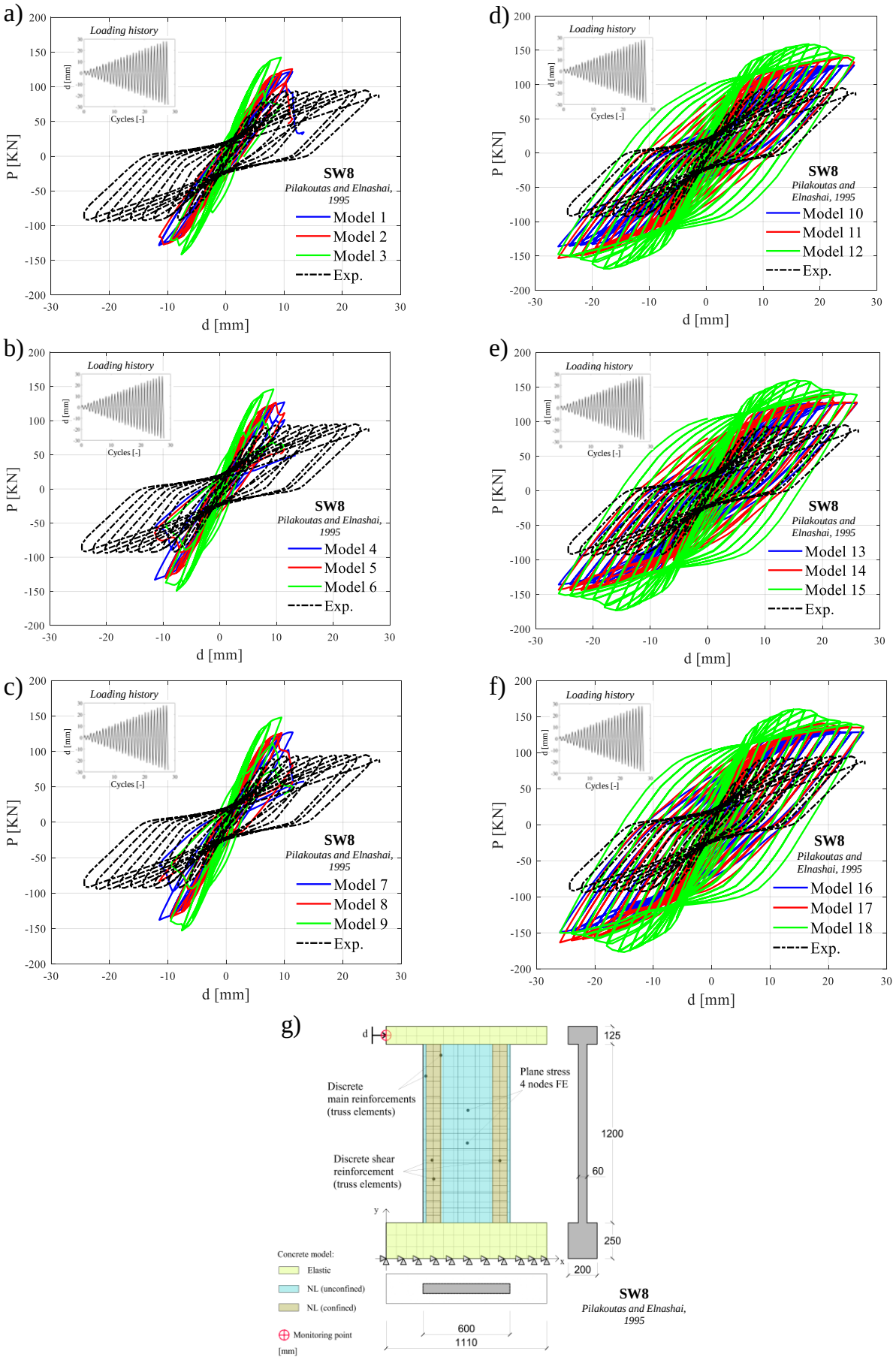

Fig. A3. Results from NLFEAs and experimental tests expressed as load vs displacement curves - SW8 of [24]; (a-c) Numerical code A, (d-f) Numerical code B. Schematization of the NLFE model (dimensions in [mm]) (g).

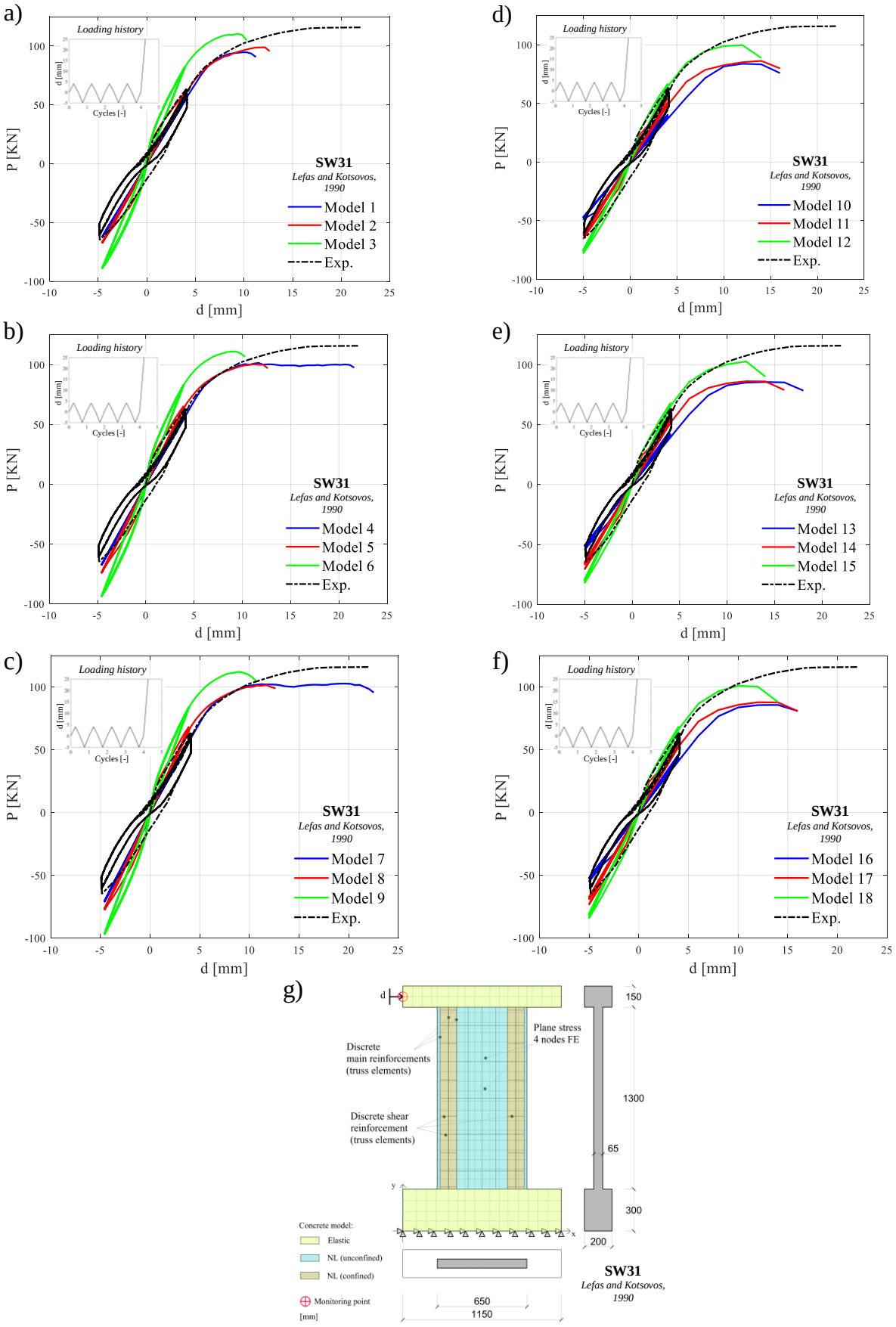

Fig. A4. Results from NLFEAs and experimental tests expressed as load vs displacement curves - SW31 of [25]; (a-c) Numerical code A, (d-f) Numerical code B. Schematization of the NLFE model (dimensions in [mm]) (g).

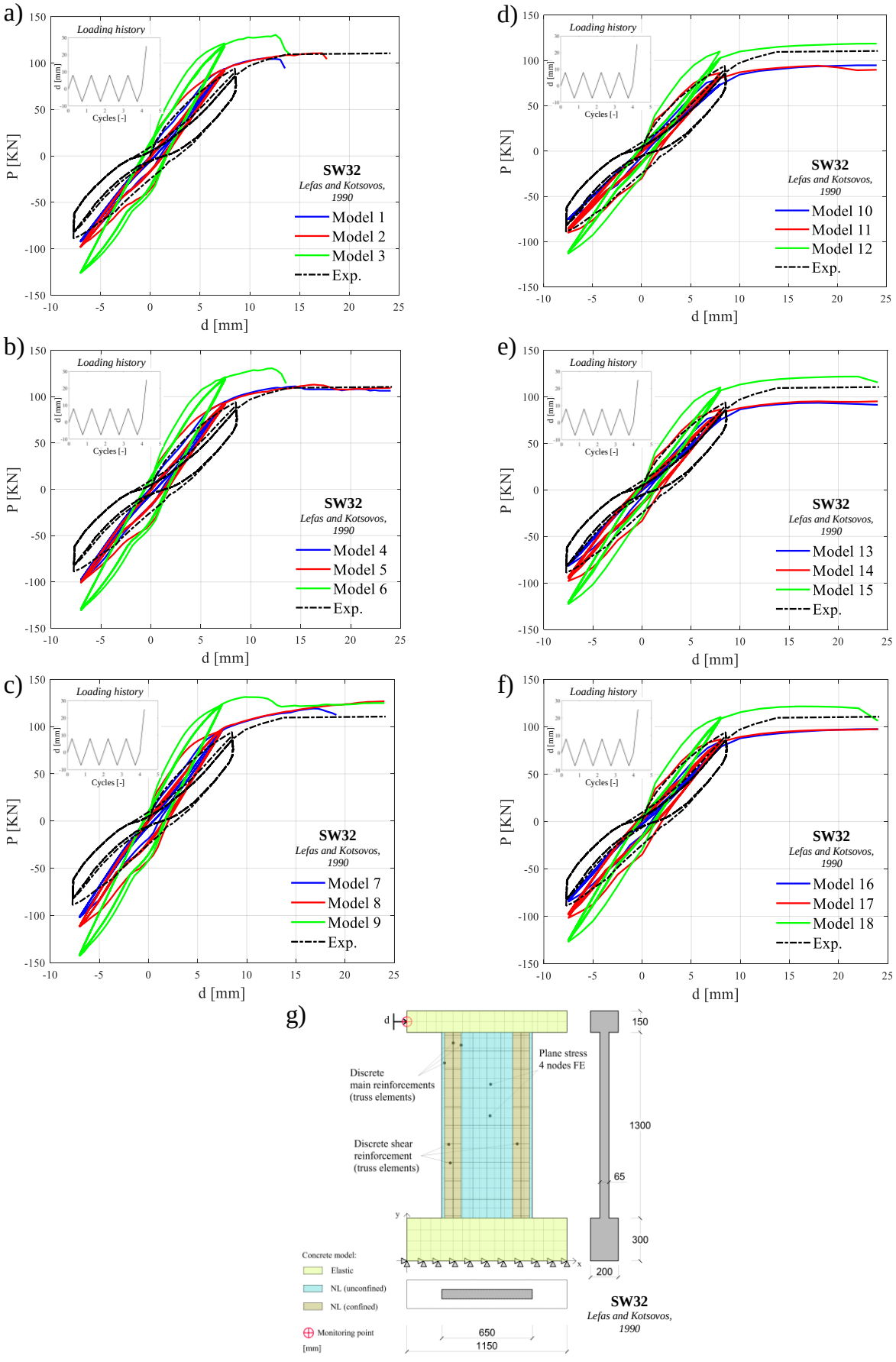

Fig. A5. Results from NLFEAs and experimental tests expressed as load vs displacement curves - SW32 of [25]; (a-c) Numerical code A, (d-f) Numerical code B. Schematization of the NLFE model (dimensions in [mm]) (g).

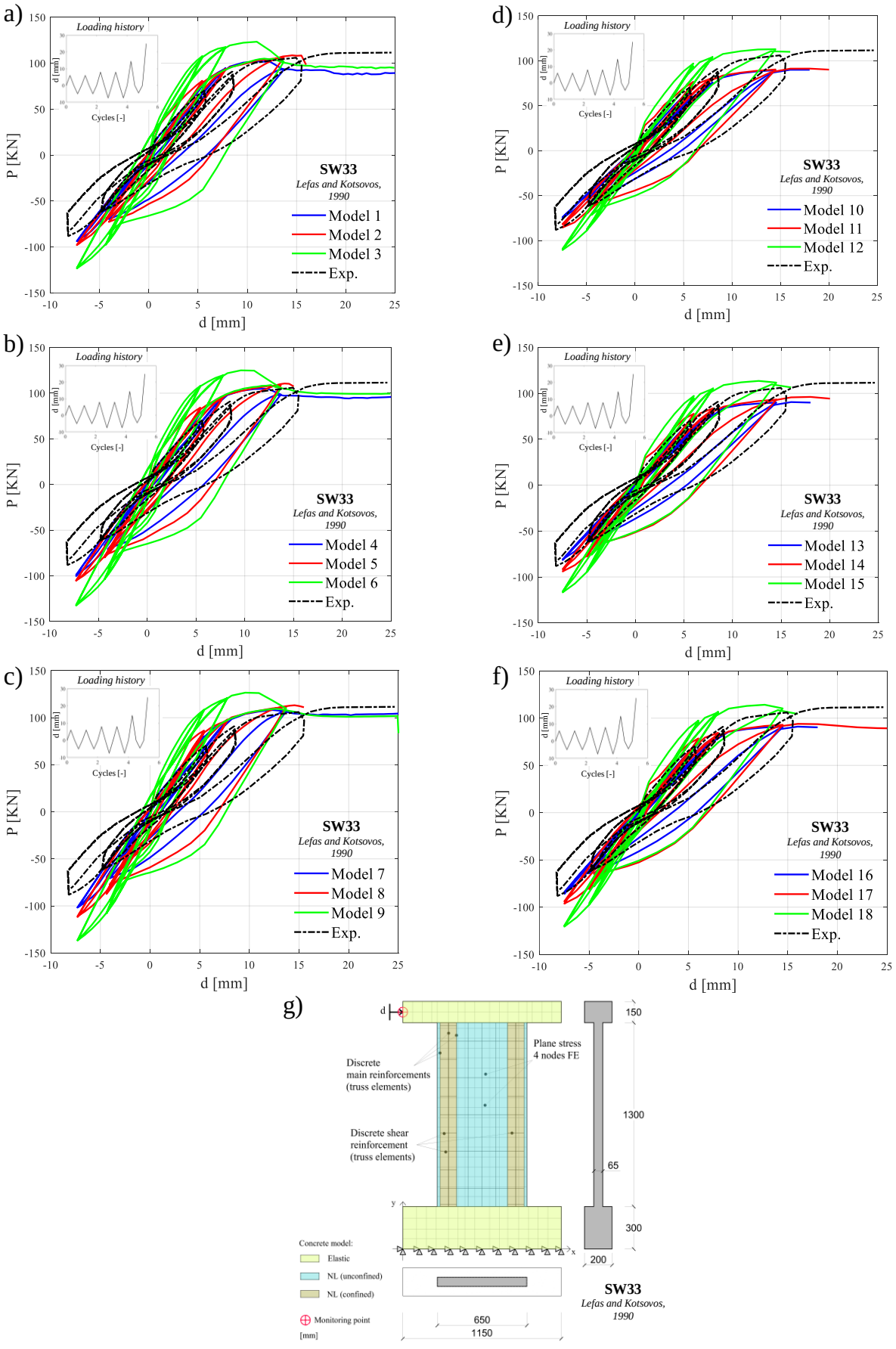

Fig. A6. Results from NLFEAs and experimental tests expressed as load vs displacement curves - SW33 of [25]; (a-c) Numerical code A, (d-f) Numerical code B. Schematization of the NLFE model (dimensions in [mm]) (g).

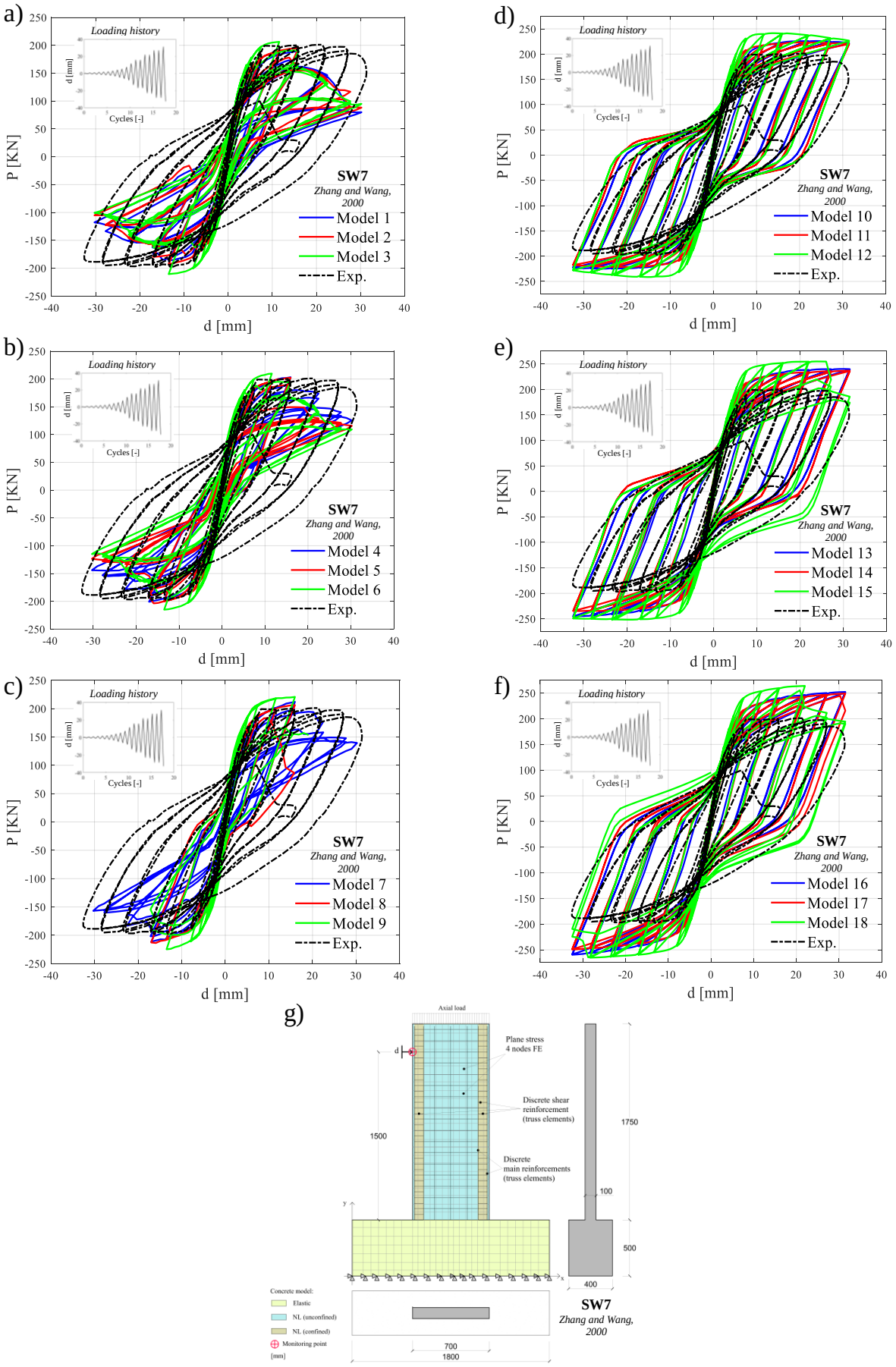

Fig. A7. Results from NLFEAs and experimental tests expressed as load vs displacement curves - SW7 of [26]; (a-c) Numerical code A, (d-f) Numerical code B. Schematization of the NLFE model (dimensions in [mm]) (g).

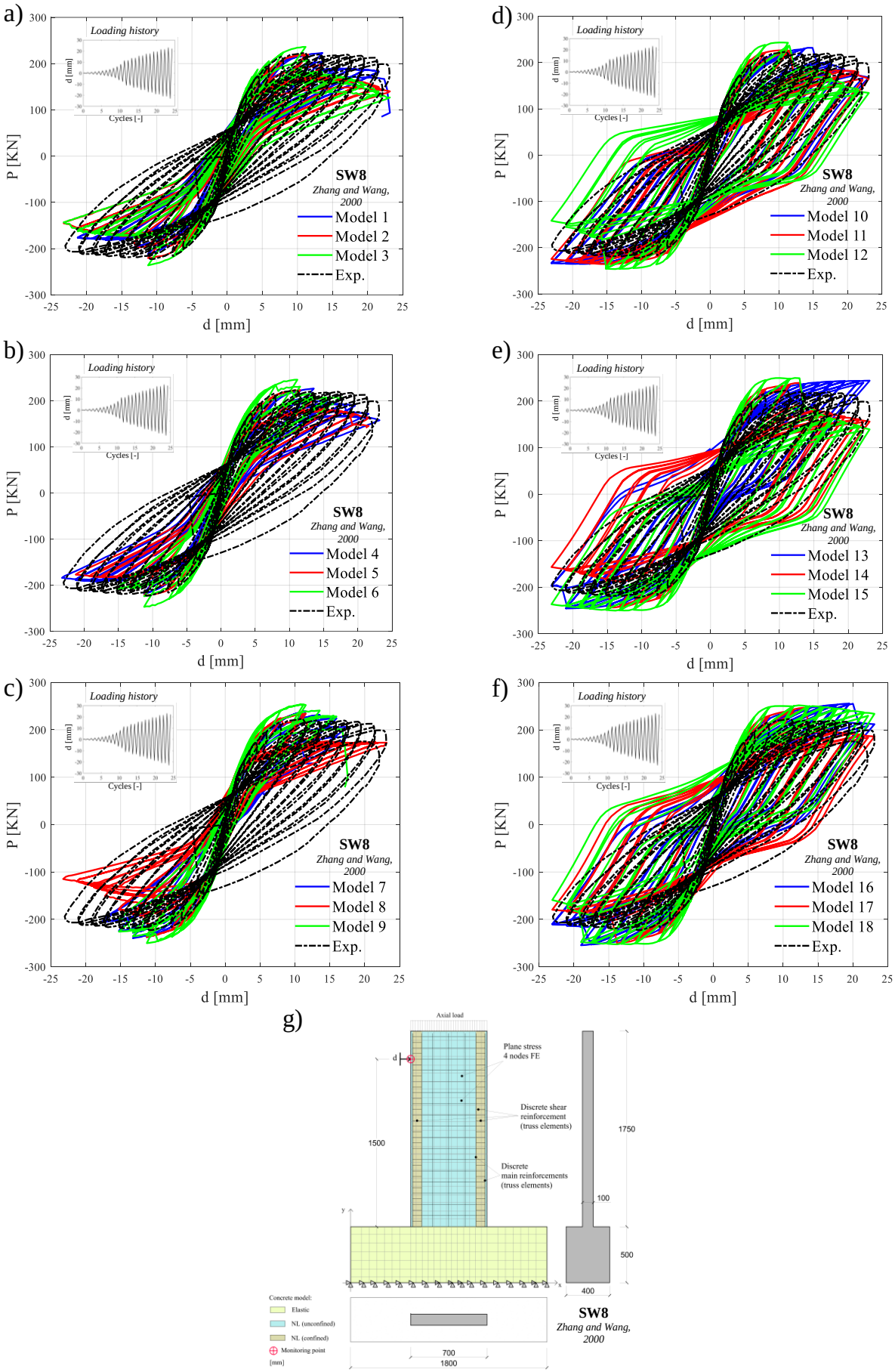

Fig. A8. Results from NLFEAs and experimental tests expressed as load vs displacement curves - SW8 of [26]; (a-c) Numerical code A, (d-f) Numerical code B. Schematization of the NLFE model (dimensions in [mm]) (g).

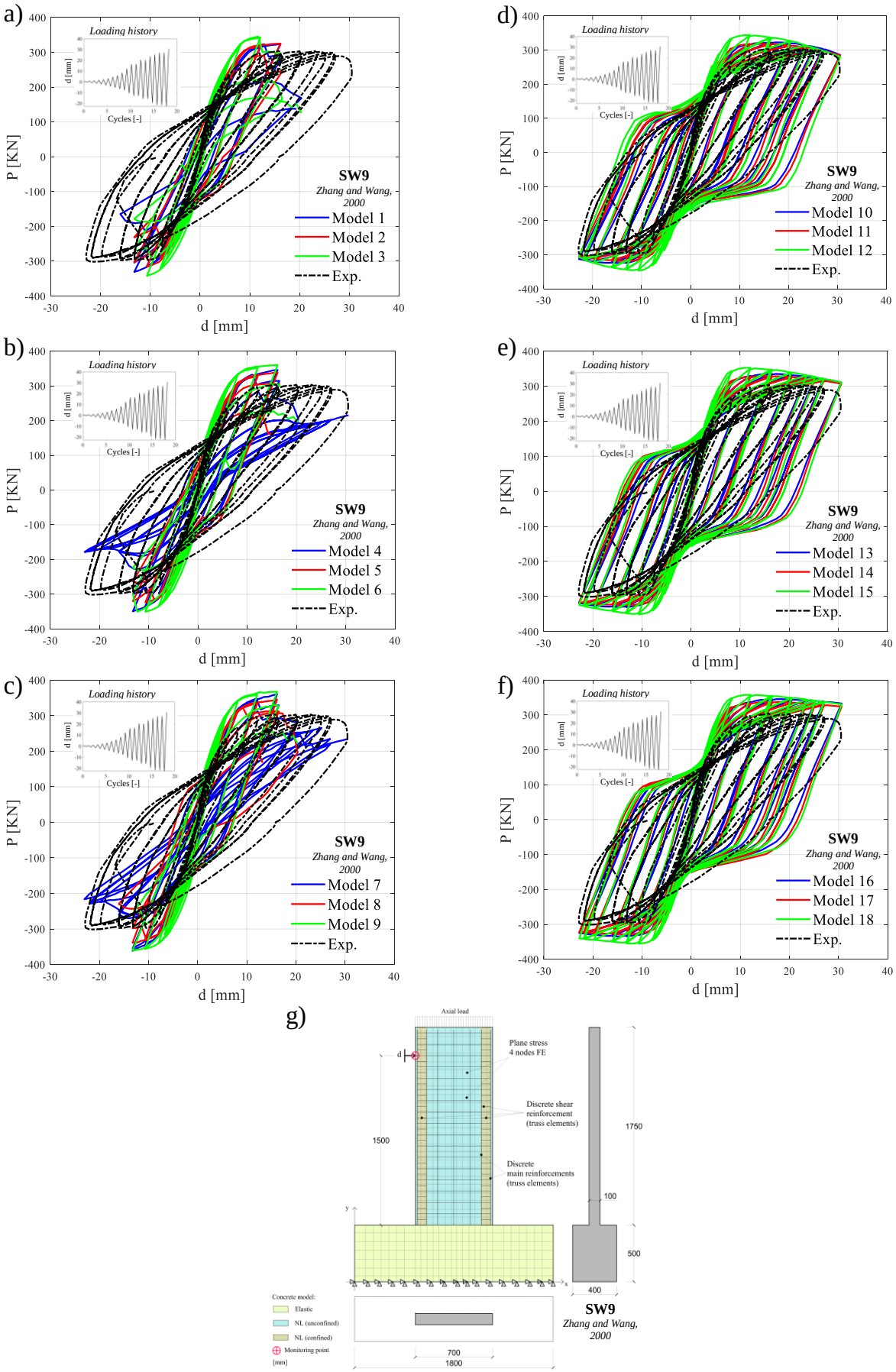

Fig. A9. Results from NLFEAs and experimental tests expressed as load vs displacement curves - SW9 of [26]; (a-c) Numerical code A, (d-f) Numerical code B. Schematization of the NLFE model (dimensions in [mm]) (g).

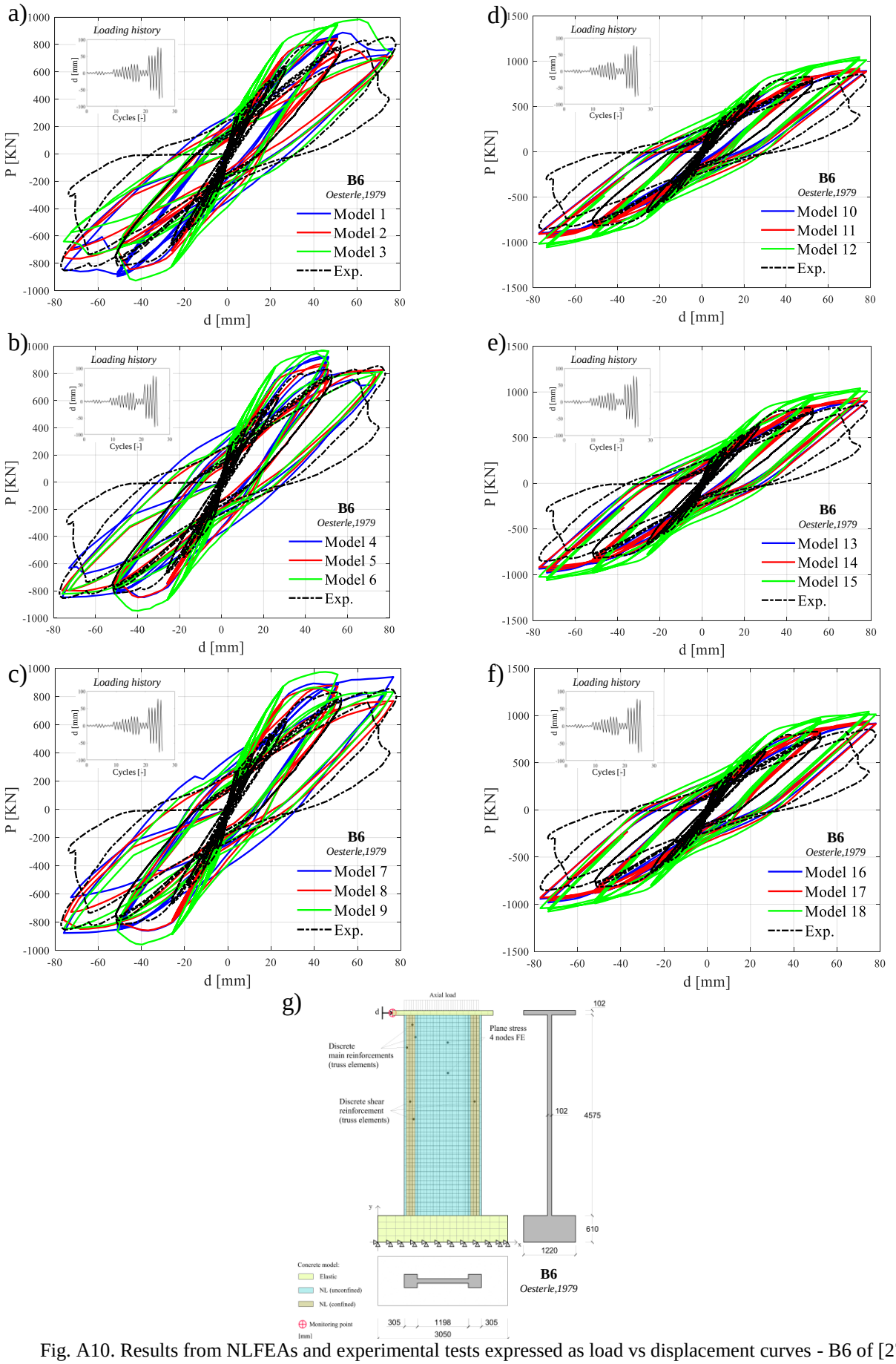

Fig. A10. Results from NLFEAs and experimental tests expressed as load vs displacement curves - B6 of [27]; (a-c) Numerical code A, (d-f) Numerical code B. Schematization of the NLFE model (dimensions in [mm]) (g).

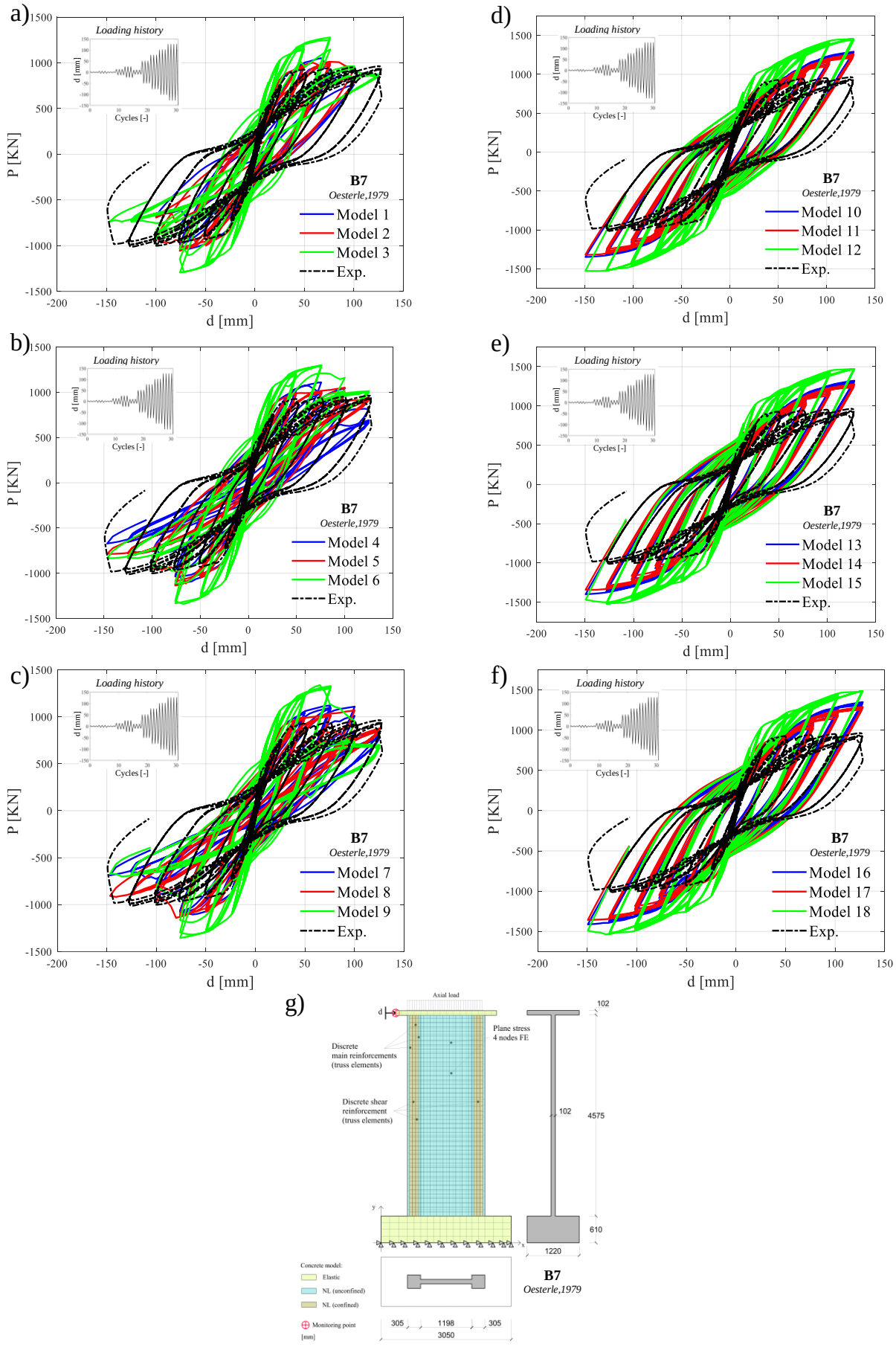

Fig. A11. Results from NLFEAs and experimental tests expressed as load vs displacement curves - B7 of [27]; (a-c) Numerical code A, (d-f) Numerical code B. Schematization of the NLFE model (dimensions in [mm]) (g).

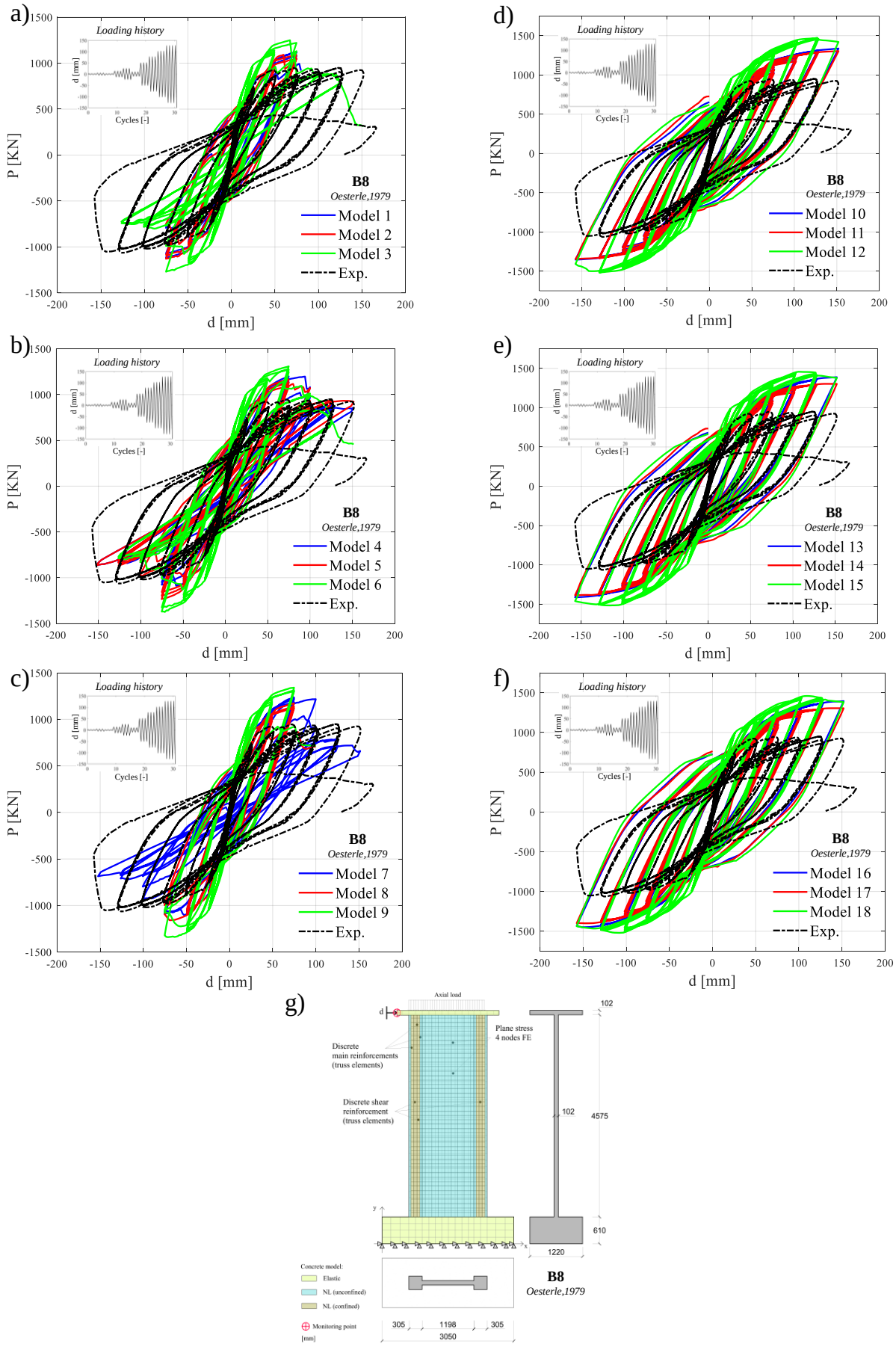

Fig. A12. Results from NLFEAs and experimental tests expressed as load vs displacement curves - B8 of [27]; (a-c) Numerical code A, (d-f) Numerical code B. Schematization of the NLFE model (dimensions in [mm]) (g).

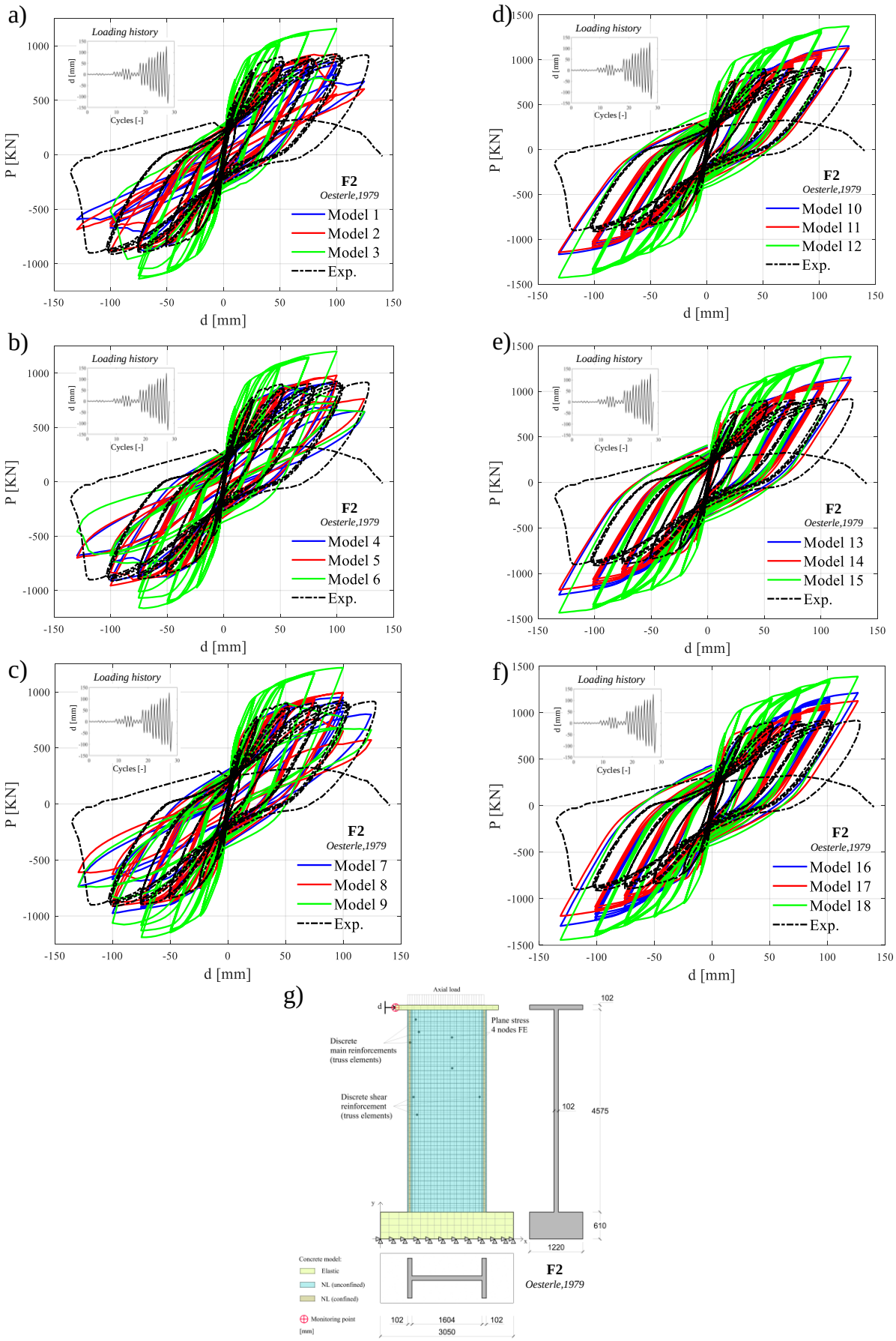

Fig. A13. Results from NLFEAs and experimental tests expressed as load vs displacement curves - F2 of [27]; (a-c) Numerical code A, (d-f) Numerical code B. Schematization of the NLFE model (dimensions in [mm]) (g).

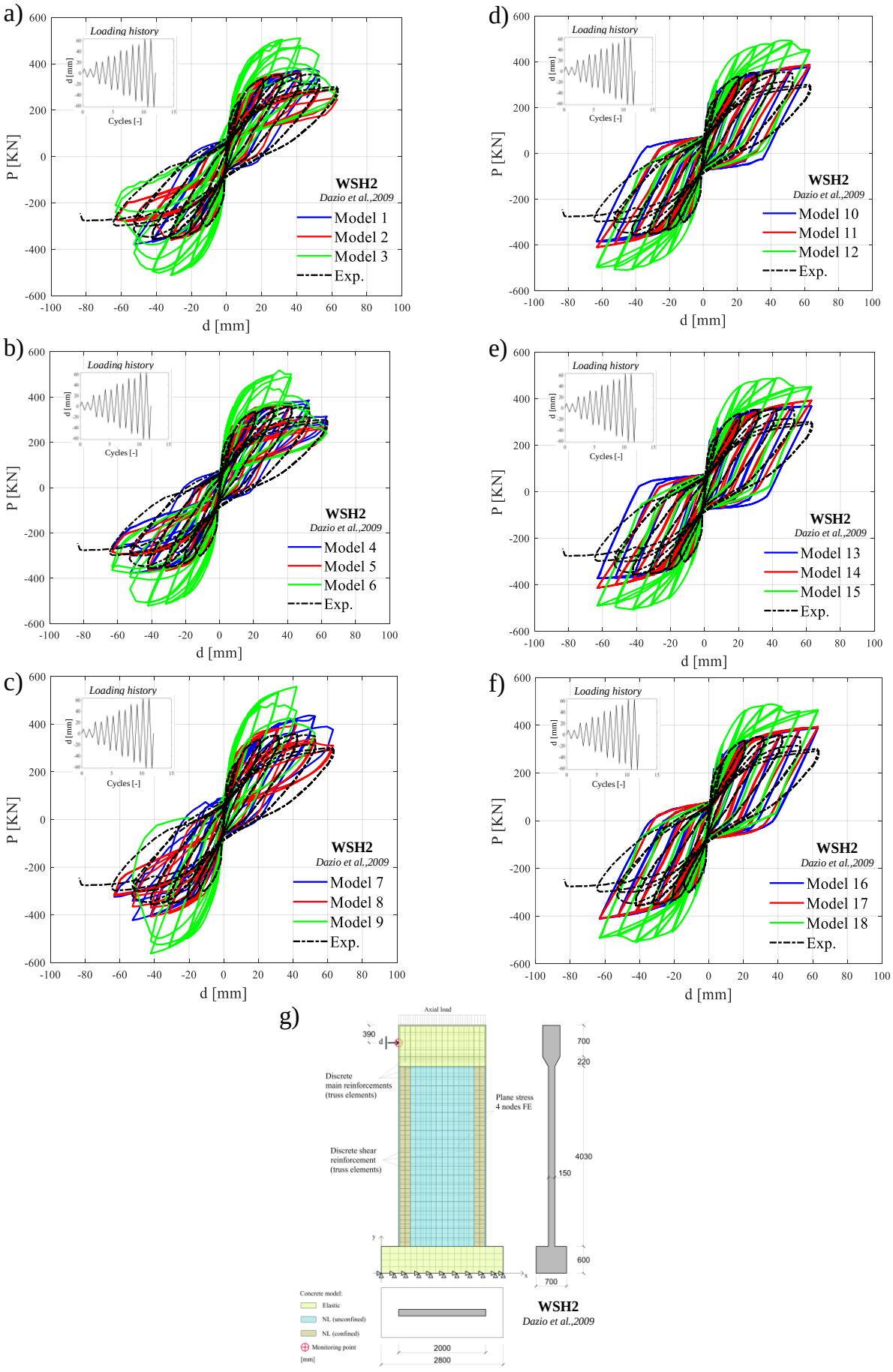

Fig. A14. Results from NLFEAs and experimental tests expressed as load vs displacement curves - WSH2 of [28]; (a-c) Numerical code A, (d-f) Numerical code B. Schematization of the NLFE model (dimensions in [mm]) (g).

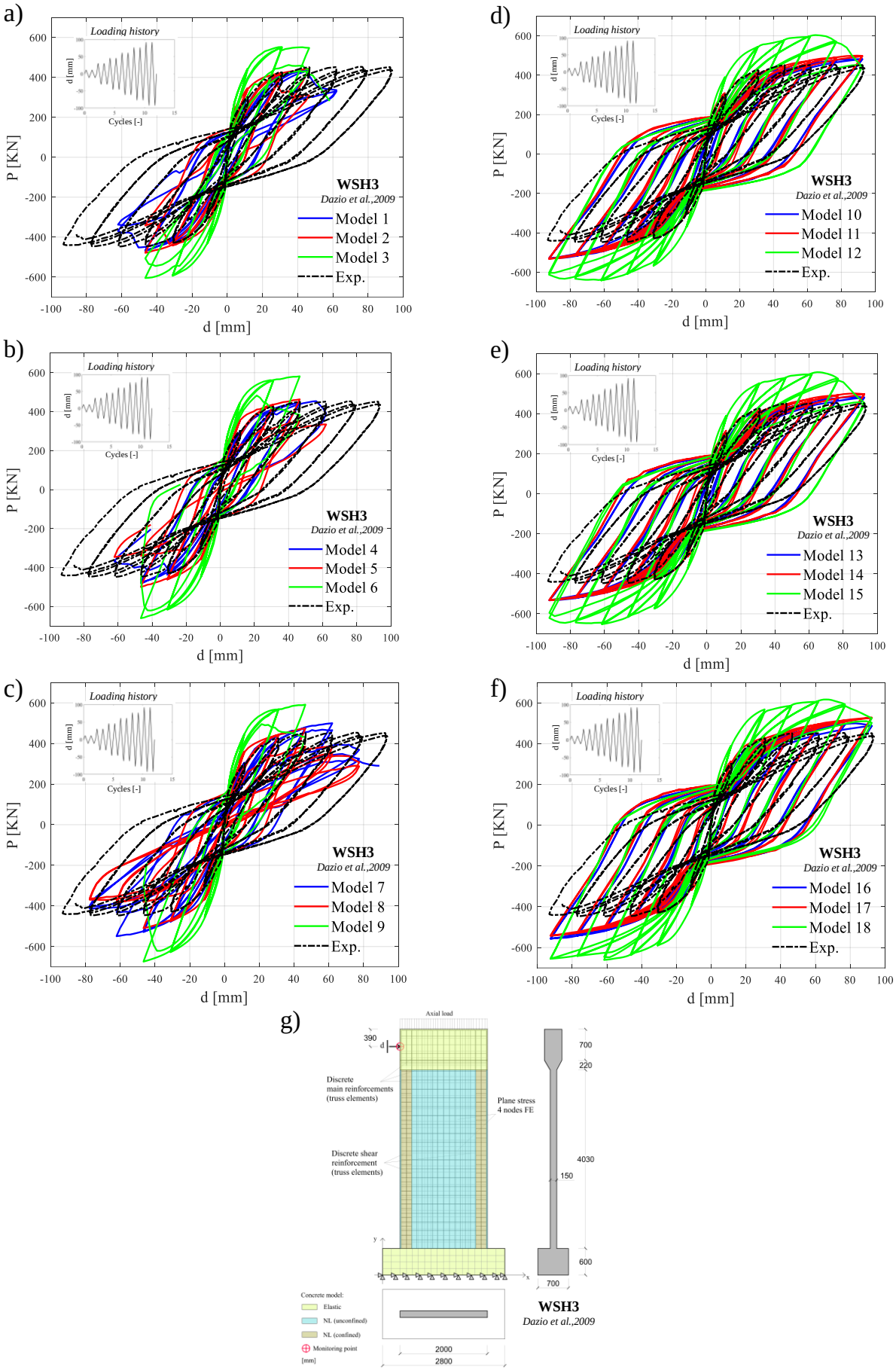

Fig. A15. Results from NLFEAs and experimental tests expressed as load vs displacement curves - WSH3 of [28]; (a-c) Numerical code A, (d-f) Numerical code B. Schematization of the NLFE model (dimensions in [mm]) (g).

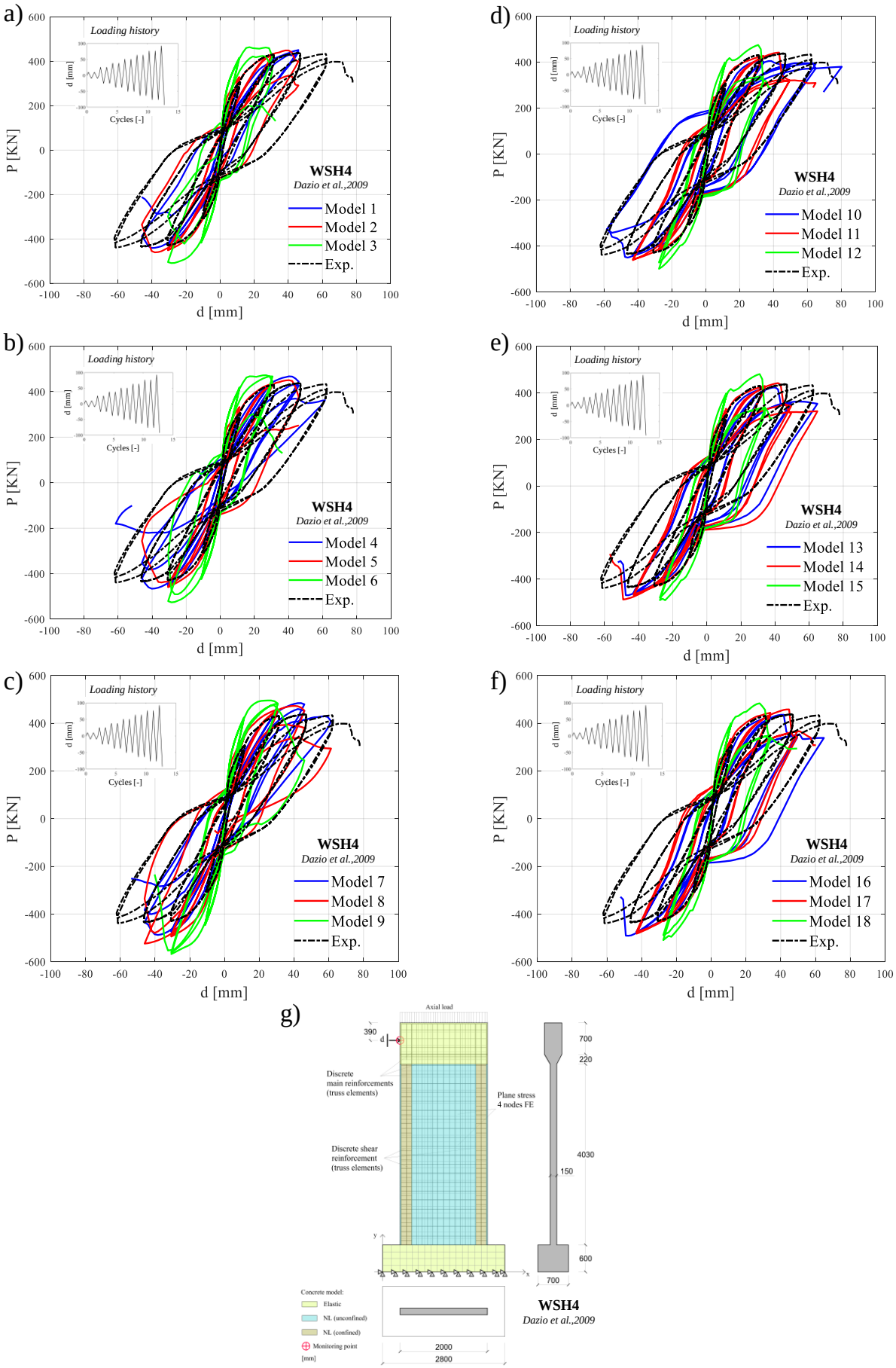

Fig. A16. Results from NLFEAs and experimental tests expressed as load vs displacement curves - WSH4 of [28]; (a-c) Numerical code A, (d-f) Numerical code B. Schematization of the NLFE model (dimensions in [mm]) (g).

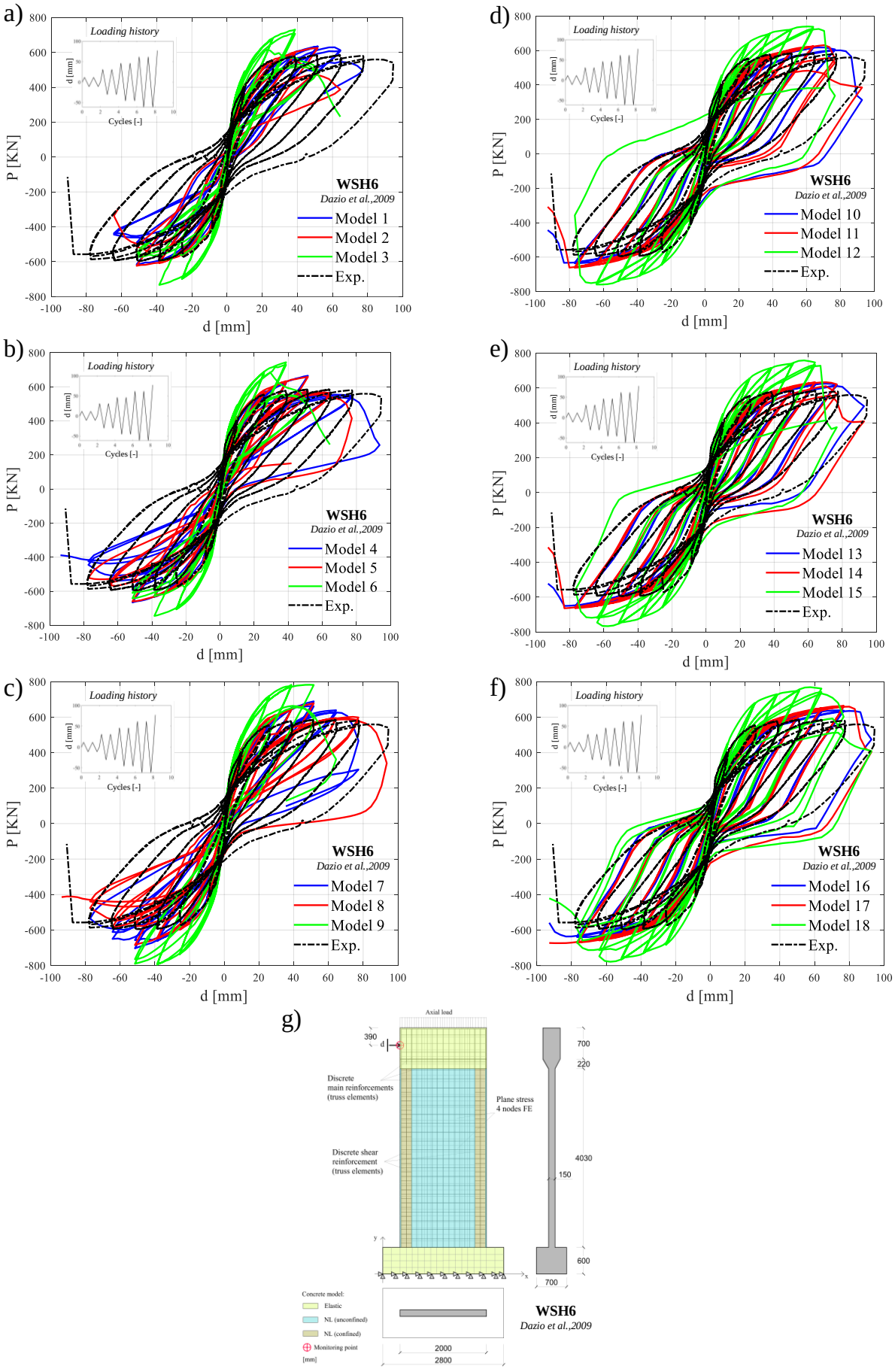

Fig. A17. Results from NLFEAs and experimental tests expressed as load vs displacement curves - WSH6 of [28]; (a-c) Numerical code A, (d-f) Numerical code B. Schematization of the NLFE model (dimensions in [mm]) (g).

Table A1. Numerical modelling for the experimental tests [24]: data concerning average mesh sizes, ratio of maximum tensile deformation of concrete $\varepsilon_{ct,LTS}$ to deformation at peak tensile concrete strength ε_{ct} and shear retention factor β.

Ref. [*]	Property	Exp. test	Modelling hypothesis																	
			M_1	M_2	M_3	M_4	M_5	M_6	M_7	M_8	M_9	M_{10}	M_{11}	M_{12}	M_{13}	M_{14}	M_{15}	M_{16}	M_{17}	M_{18}
[24]	Average mesh size [cm]	SW4 SW6 SW8	5.0x5.0																	
	$\varepsilon_{ct,LTS}/\varepsilon_{ct}$ [-]	SW4	*Brittle*	10.0	*Plastic*	*Brittle*	8.6	*Plastic*	*Brittle*	10.0	*Plastic*	*Brittle*	9.7	*Plastic*	*Brittle*	10.0	*Plastic*	*Brittle*	10.0	*Plastic*
		SW6		9.5			9.0			9.5			10.0			9.8			10.0	
		SW8		9.5			10.0			10.0			9.2			9.5			9.1	
	β [-]	SW4	0.10			0.20	0.15	0.14	0.30			0.10			0.19	0.15	0.20	0.30		
		SW6				0.12	0.20	0.12							0.20	0.19	0.20			
		SW8				0.19	0.20	0.18							0.20	0.21	0.19			

Table A2. Numerical modelling for the experimental tests [25]: data concerning average mesh sizes, ratio of maximum tensile deformation of concrete $\varepsilon_{ct,LTS}$ to deformation at peak tensile concrete strength ε_{ct} and shear retention factor β.

Ref. [*]	Property	Exp. test	Modelling hypothesis																	
			M_1	M_2	M_3	M_4	M_5	M_6	M_7	M_8	M_9	M_{10}	M_{11}	M_{12}	M_{13}	M_{14}	M_{15}	M_{16}	M_{17}	M_{18}
[25]	Average mesh size [cm]	SW31 SW32 SW33	5.0x5.0																	
	$\varepsilon_{ct,LTS}/\varepsilon_{ct}$ [-]	SW31	*Brittle*	9.6	*Plastic*	*Brittle*	10.0	*Plastic*	*Brittle*	9.8	*Plastic*	*Brittle*	9.4	*Plastic*	*Brittle*	9.1	*Plastic*	*Brittle*	9.8	*Plastic*
		SW32		8.5			8.2			7.9			9.4			8.9			9.5	
		SW33		10.0			9.5			8.6			9.5			9.1			9.2	
	β [-]	SW31	0.10			0.22	0.20	0.20	0.30			0.10			0.19	0.20	0.21	0.30		
		SW32				0.20	0.12	0.21							0.21	0.20	0.20			
		SW33				0.20	0.21	0.22							0.18	0.20	0.21			

Table A3. Numerical modelling for Experimental tests [26]: data concerning average mesh sizes, ratio of maximum tensile deformation of concrete $\varepsilon_{ct,LTS}$ to deformation at peak tensile concrete strength ε_{ct} and shear retention factor β.

Ref. [*]	Property	Exp. test	Modelling hypothesis																	
			M_1	M_2	M_3	M_4	M_5	M_6	M_7	M_8	M_9	M_{10}	M_{11}	M_{12}	M_{13}	M_{14}	M_{15}	M_{16}	M_{17}	M_{18}
[26]	Average mesh size [cm]	SW31 SW32 SW33	5.0x5.0																	
	$\varepsilon_{ct,LTS}/\varepsilon_{ct}$ [-]	SW31	*Brittle*	8.0	*Plastic*	*Brittle*	8.4	*Plastic*	*Brittle*	9.1	*Plastic*	*Brittle*	8.4	*Plastic*	*Brittle*	9.4	*Plastic*	*Brittle*	9.5	*Plastic*
		SW32		9.5			9.1			8.5			9.2			9.7			9.1	
		SW33		10.0			9.4			9.3			9.5			9.6			9.1	
	β [-]	SW31	0.10			0.20	0.21	0.12	0.30			0.10			0.17	0.20	0.19	0.30		
		SW32				0.12	0.13	0.20							0.21	0.19	0.20			
		SW33				0.21	0.20	0.19							0.21	0.22	0.19			

Table A4. Numerical modelling for the experimental tests [27]: data concerning average mesh sizes, ratio of maximum tensile deformation of concrete $\varepsilon_{ct,LTS}$ to deformation at peak tensile concrete strength ε_{ct} and shear retention factor β.

Ref. [*]	Property	Exp. test	Modelling hypothesis																	
			M_1	M_2	M_3	M_4	M_5	M_6	M_7	M_8	M_9	M_{10}	M_{11}	M_{12}	M_{13}	M_{14}	M_{15}	M_{16}	M_{17}	M_{18}
[27]	Average mesh size [cm]	B6 B7 B8 F2	10.2x10.2 12.0x12.0 10.0x10.0 5.0x5.0																	
	$\varepsilon_{ct,LTS}/\varepsilon_{ct}$ [-]	B6	*Brittle*	5.9	*Plastic*	*Brittle*	6.5	*Plastic*	*Brittle*	6.4	*Plastic*	*Brittle*	5.8	*Plastic*	*Brittle*	6.1	*Plastic*	*Brittle*	6.4	*Plastic*
		B7		7.5			7.8			6.7			8.1			8.2			9.1	
		B8		9.5			9.6			9.3			9.1			8.9			8.8	
		F2		9.8			9.5			8.9			9.1			8.6			8.4	
	β [-]	B6	0.10			0.20	0.15	0.19	0.30			0.10			0.20	0.14	0.21	0.30		
		B7				0.21	0.22	0.20							0.22	0.20	0.19			
		B8				0.20	0.22	0.20							0.21	0.21	0.22			
		F2				0.23	0.20	0.20							0.19	0.20	0.21			

Table A5. Numerical modelling for the experimental tests [28]: data concerning average mesh sizes, ratio of maximum tensile deformation of concrete $\varepsilon_{ct,LTS}$ to deformation at peak tensile concrete strength ε_{ct} and shear retention factor β.

Ref. [*]	Property	Exp. test	Modelling hypothesis																	
			M_1	M_2	M_3	M_4	M_5	M_6	M_7	M_8	M_9	M_{10}	M_{11}	M_{12}	M_{13}	M_{14}	M_{15}	M_{16}	M_{17}	M_{18}
[28]	Average mesh size [cm]	WSH2	10.0x10.0																	
		WSH3																		
		WSH4																		
		WSH6	12.0x12.0																	
	$\varepsilon_{ct,LTS}/\varepsilon_{ct}$ [-]	WSH2	*Brittle*	7.2	*Plastic*	*Brittle*	7.3	*Plastic*	*Brittle*	8.1	*Plastic*	*Brittle*	8.5	*Plastic*	*Brittle*	8.4	*Plastic*	*Brittle*	9.1	*Plastic*
		WSH3		9.5			8.4			7.5			9.4			8.1			8.0	
		WSH4		9.1			6.4			7.2			8.9			7.2			8.1	
		WSH6		5.3			5.8			6.3			5.6			4.9			6.1	
	β [-]	WSH2	0.10			0.12	0.13	0.12	0.30			0.10			0.13	0.12	0.19	0.30		
		WSH3				0.13	0.12	0.20							0.13	0.12	0.12			
		WSH4				0.20	0.12	0.14							0.12	0.13	0.13			
		WSH6				0.19	0.20	0.12							0.13	0.12	0.12			

REFERENCES

[1] *fib* Bulletin N°45. Practitioner's guide to finite element modelling of reinforced concrete structures – State of the art report. Lausanne; 2008.
[2] Belletti B, Damoni C, Hendriks MAN. Development of guidelines for nonlinear finite element analyses of existing reinforced and prestressed beams. European Journal of Environmental and Civil Engineering 2011;15(9): 1361-1384.
[3] DNV-RP-C208. Determination of structural capacity by non-linear FE analysis methods, Recommended Practice, DET NORSKE VERITAS AS 2013, http://www.dnv.com.
[4] Most T. Assessment of structural simulation models by estimating uncertainties due to model selection and model simplification. Computers and Structures 2011; 89(17-18): 1664-1672.
[5] *fib* Model Code for Concrete Structures 2010. fib 2013. Lausanne.
[6] CEN. EN 1990: Eurocode – Basis of structural design. CEN 2013. Brussels.
[7] ISO 2394. General principles on reliability for structures. Genéve. 1998.
[8] ISO 2394. General principles on reliability for structures. Genéve. 2015.
[9] *fib* Bulletin N°80. Partial factor methods for existing concrete structures, Lausanne, Switzerland; 2016.
[10] Allaix DL, Carbone VI, Mancini G. Global safety format for non-linear analysis of reinforced concrete structures. Structural Concrete 2013; 14(1): 29-42.
[11] Shlune H, Gylltoft K, Plos M. Safety format for non-linear analysis of concrete structures. Magazine of Concrete Research 2012; 64(7): 563-574.
[12] König G, Nguyen T, Ahner C. Consistent safety format. In: CEB, editor. CEB bulletin 239 – non-linear analysis: discussion papers from the working party in commission 1. CEB 1997. Lausanne.
[13] Ftima MB, Massicotte B. Development of a reliability framework for the use of advanced nonlinear finite elements in the design of concrete structures. Journal of Structural Engineering 2012; 138:1054–64.
[14] CEN EN 1992-2 Eurocode 2 – Design of concrete structures, Part 2: concrete bridges. CEN 2005. Brussels.
[15] Blomfors M, Engen M, Plos M. Evaluation of safety formats for non-linear finite element analyses of statically indeterminate concrete structures subjected to different load paths. Structural Concrete 2016; 17(1): 44-51.
[16] Val D, Bljuger F, Yankelevsky D. Reliability evaluation in nonlinear analysis of reinforced concrete structures. Structural Safety 1997; 19(2): 203-217.
[17] Cervenka V. Global safety formats in *fib* Model Code 2010 for design of concrete structures. Proceedings of the 11th International Probabilistic Workshop, Brno, 2013.
[18] Cervenka V. Reliability-based non-linear analysis according to fib Model Code 2010. Structural Concrete 2013; 14(1): 19-28.
[19] Castaldo, P., Gino, D., Mancini, G. (2019) Safety formats for non-linear finite element analysis of reinforced concrete structures: discussion, comparison and proposals, Engineering Structures, 193, pp. 136-153.
[20] Castaldo, P., Gino, D., Bertagnoli, G., Mancini, G. (2018) Partial safety factor for resistance model uncertainties in 2D non-linear finite element analysis of reinforced concrete structures, Engineering Structures, 176, pp. 746-762.
[21] JCSS. JCSS Probabilistic Model Code. 2001.
[22] Kadlec L, Červenka V. Model Uncertainties of FEM Nonlinear Analyses of Concrete Structures. Solid State Phenomena 2016; 249: 197-202.
[23] Engen M, Hendriks MAN, Köhler J, Øverli JA, Åldtstedt E. A quantification of modelling uncertainty for non-linear finite element analysis of large concrete structures. Structural Safety 2017; 64: 1-8.

[24] Kypros Pilakoutas and Amr Einashai. Cyclic Behaviour of Reinforced Concrete Cantilever Walls, Part I : Experimental Results. ACI structural journal no.92-S25, 1995.
[25] Ioannis D. Lefas and Micheal D. Kotsovos. Strength and deformation characteristics of reinforced concrete walls under load reversals. ACI structural journal no.87-S74, 1990.
[26] Yunfeng Zhang and Zhihao Wang. Seismic behaviour of reinforced concrete shear walls subjected to high axial loading. ACI structural journal no.97-S75, 2000.
[27] R.G. Oesterle, et al. Earthquake resistant structural walls - Tests of isolated walls - Phase II. Portland cement association, 1979.
[28] A. Dazio et al. Quasi-static cyclic tests and plastic hinge analysis of RC structural walls. Engineering Structures 31: 1556-1571, 2009.
[29] Almeida, J., Prodan, O., Rosso, A., Beyer, K. Tests on thin reinforced concrete walls subjected to in-plane and out-of-plane cyclic loading. Earthquake Spectra. Volume 33, Issue 1, 2017, Pages 323-345.
[30] Dashti, F., Dhakal, R.P., Pampanin, S. A parametric investigation on applicability of the curved shell finite element model to nonlinear response prediction of planar RC walls. Bulletin of Earthquake Engineering. Volume 17, Issue 12, 1 December 2019, Pages 6515-6546.
[31] Belletti B., Scolari M., Almeida J., Beyer K. Validation of NLFEA to simulate the instability of thin RC walls subjected to bidirectional loading. Lecture Notes in Civil Engineering 10: 32-48.
[32] Kiureghian AD, Ditlevsen O. Aleatory or epistemic? Does it matter?. Structural Safety 2009; 31: 105-112.
[33] Patè-Cornell ME. Uncertainties in risk analysis: six levels of treatment, Reliability Engineering and System Safety 1996; 54: 95-111.
[34] Ditlevsen O. Model uncertainty in structural reliability. Structural Safety 1982; 1: 73-86.
[35] Bulleit WM. Uncertainty in structural engineering. Practice Periodical on Structural Design and Construction ASCE 2008; 13: 24-30.
[36] CEN. EN 1992-1-1: Eurocode 2 – Design of concrete structures. Part 1-1: general rules and rules for buildings. CEN 2014. Brussels.
[37] Allen TM , Nowak AS, Bathurst RJ. Calibration to determine load and resistance factor for geotechnical a structural design. Transport research board circular N° EC-079 2005. Washington.
[38] Holický M, Retief JV, Sikora M. Assessment of model uncertainties for structural resistance. Probabilistic Engineering Mechanics 2016; 45: 188-197.
[39] Sykora M., Krejsa J., Mlcoch J., Prieto M., Tanner P. Uncertainty in shear resistance models of reinforced concrete beams according to *fib* MC2010, Struc. Concrete. 2018, 19(1):284-295.
[40] Sikora M, Holicky M, Prieto M, Tanner P. Uncertainties in resistance models for sound and corrosion-damaged RC structures according to EN 1992-1-1. Materials and structures 2014; 48: 3415-3430.
[41] Taerwe RL. Toward a consistent treatment of model uncertainties in reliability formats for concrete structures. CEB Bulletin d'Information 1993; 105-S17: 5-34.
[42] Hasofer AM, Lind NC. Exact and invariant second moment code format, Journal of the Engineering Division ASCE 1974; 100(EM1): 111-121.
[43] Engen M, Hendriks MAN, Øverli JA, Åldtstedt E. Solution strategy for non-linear finite element analyses of large reinforced concrete structures. Str. Concrete 2015; 3: 389-397.
[44] ATENA 2D v5. Cervenka Consulting s.r.o. . Prague. Czech Republic. 2014.
[45] DIANA FEA BV. Delftechpark 19a 2628 XJ Delft. The Netherlands. 2017.
[46] Bertagnoli G, La Mazza D, Mancini G. Effect of concrete tensile strength in non –linear analysis of 2D structures: a comparison between three commercial finite element softwares. 3rd International Conference on Advances in Civil, Structural and Construction Engineering – CSCE 2015. Rome. 104-111. 10-11 December 2015.

[47] Murat Saatcioglu and Salim R Razvi. Strength and ductility of confined concrete. Journal of Structural engineering, 118(6):1590–1607, 1992.
[48] Belletti B., Scolari M., Vecchi F. PARC_CL 2.0 crack model for NLFEA of reinforced concrete structures under cyclic loadings. Computer and Structures 191: 165-179.
[49] De Borst R, Nauta P. Non-orthogonal cracks in a smeared finite element model. Engineering Computations 1985; 2: 35-46.
[50] Menegotto, M. and Pinto, E. (1973), Method of analysis for cyclically loaded reinforced concrete plane frames including changes in geometry and non-elastic behavior of elements under combined normal force and bending, ‖ Proceedings, IABSE Symposium. Lisbon, Portugal.
[51] Riggs HR, Powell GH. Rough crack model for analysis of concrete. J. Eng. Mech. Div. ASCE 1986; 112(5): 448-464.
[52] Kupfer, H. B. and Gerstle, H. K. (1973). Behavior of Concrete under Biaxial Stresses. Journal Engineering Mechanics Division 99(4).
[53] Massicotte B, Elwi AE, MacGregor JG. Tension-stiffening models for planar reinforced concrete members. Journal of Structural Engineering 199; 116(11): 3039-3058.
[54] D.L.Araújo, et al. Computational modelling of steel fibre reinforced Concrete beams subjected to shear. IBRACON Structures and Materials Journal, vol. 3 n1, 2010.
[55] S. Matsuoka, et al. ANALITICAL MODEL FOR CONCRETE STRUCTURES INFLUENCED BY CRACK initiation and propagation. Concrete Library of JSCE no.35, 2000.
[56] E. Fehiling and T. Bullo. Ultimate load capacity of reinforcement steel fibre concrete deep beams subjected to shear. Finite elements in Civil Engineering Applications, Hendriks & Rots, 2002.
[57] N. Shirai, et al. Finite element analysis of shear wall specimens made of ductile fibre reinforced cementitious composites subjected to lateral loading. Finite elements in Civil Engineering Applications, Hendriks & Rots, 2002.
[58] X.Zhang and D.Wang. Influence of the shear retention factor on the fracture behaviour of fibre reinforced concrete. Advances in Materials Sciences, Energy Technology and Environmental Engineering, 2017.
[59] Comité euro-international du béton. RC Elements Under Cyclic Loading: State of the Art Report, 1996.
[60] Park R. Ductility evaluation from laboratory and analytical testing. In: Proceedings of the 9th world conference on earthquake engineering. Vol. III; 1988.
[61] Gelman A, Carlin JB, Stern HS, Dunson DB, Vehtari A, Rubin DB. Bayesian data analysis. 3rd ed. CRC Press; 2014.
[62] Faber, Michael Havbro Statistics and Probability Theory, Springer, 2012.
[63] Castaldo P., Gino D., Carbone V.I., Mancini G. (2018) Framework for definition of design formulations from empirical and semi-empirical resistance models, Structural Concrete 19(4): 980-987.
[64] Caspeele R, Sýkora M, Allaix DL, Steenbergen R. The design value method and adjusted partial factor approach for existing structures. Structural Engineering International, 23(4):386–393. 2013.